The ubiquitin-specific protease USP8 is critical for the development and homeostasis of T cells

Dufner, Almut ; Kisser, Agnes ; Niendorf, Sandra ; Basters, Anja ; Reissig, Sonja ; Schönle, Anne ; Aichem, Annette ; Kurz, Thorsten ; Schlosser, Andreas ; Yablonski, Deborah ; Groettrup, Marcus ; Buch, Thorsten ; Waisman, Ari ; Schamel, Wolfgang W ; Prinz, Marco ; Knobeloch, Klaus-Peter

Abstract: The modification of proteins by ubiquitin has a major role in cells of the immune system and is counteracted by various deubiquitinating enzymes (DUBs) with poorly defined functions. Here we identified the ubiquitin-specific protease USP8 as a regulatory component of the T cell antigen receptor (TCR) signalosome that interacted with the adaptor Gads and the regulatory molecule 14-3-3 . Caspase-dependent processing of USP8 occurred after stimulation of the TCR. T cell-specific deletion of USP8 in mice revealed that USP8 was essential for thymocyte maturation and upregulation of the gene encoding the cytokine receptor IL-7R mediated by the transcription factor Foxo1. Mice with T cell-specific USP8 deficiency developed colitis that was promoted by disturbed T cell homeostasis, a predominance of CD8(+) T cells in the intestine and impaired regulatory T cell function. Collectively, our data reveal an unexpected role for USP8 as an immunomodulatory DUB in T cells.

DOI: https://doi.org/10.1038/ni.3230

Ubiquitin-specific protease 8 (USP8) is a GADS interacting component of the T-cell receptor signalosome and critical for T-cell development and homeostasis

Almut Dufner[1], Agnes Kisser[2,12], Sandra Niendorf[2,13], Anja Basters[1], Sonja Reissig[3], Anne Schönle[1], Annette Aichem[4], Thorsten Kurz[5], Andreas Schlosser[5,14], Deborah Yablonski[6], Marcus Groettrup[4,7], Thorsten Buch[8,9], Ari Waisman[3], Wolfgang W. Schamel[10,11], Marco Prinz[1,11], and Klaus-Peter Knobeloch[1,2]

[1]Institute of Neuropathology, University of Freiburg, Freiburg, Germany

[2]Leibniz Institute for Molecular Pharmacology (FMP), Berlin, Germany

[3]Institute for Molecular Medicine, University Medical Center of the Johannes Gutenberg University of Mainz, Mainz, Germany

[4]Biotechnology Institute Thurgau at the University of Konstanz, Kreuzlingen, Switzerland

[5]Center for Biological Systems Analysis, University of Freiburg, Freiburg, Germany

[6]Ruth and Bruce Rappaport Faculty of Medicine, Technion-Israel Institute of Technology, Haifa, Israel

[7]Division of Immunology, Department of Biology, University of Konstanz, Konstanz, Germany

[8]Institute for Medical Microbiology, Immunology, and Hygiene, Technische Universität München, Germany

[9]Institute of Laboratory Animal Sciences, University of Zurich, Switzerland

[10]Department of Molecular Immunology, Faculty of Biology, and Center of Chronic Immunodeficiency (CCI), University of Freiburg, Freiburg, Germany

[11]BIOSS Center for Biological Signaling Studies, University of Freiburg, Freiburg, Germany

[12]Current address: Ludwig Boltzmann Institute for Health Technology Assessment, Vienna, Austria

[13]Current address: Department of Infectious Diseases, Robert Koch Institute, Berlin, Germany

[14]Current address: Rudolf-Virchow-Zentrum für Experimentelle Biomedizin, Würzburg, Germany

Correspondence should be addressed to K.-P.K. klaus-peter.knobeloch@uniklinik-freiburg.de or A.D. almut.dufner@uniklinik-freiburg.de

Abstract

Ubiquitin-modification is counteracted by deubiquitinating enzymes (DUBs). Here we identify USP8 as a novel component of the TCR signalosome that interacts with the adapter molecule GADS and 14-3-3β. Upon TCR-stimulation USP8 is processed in a caspase-dependent manner. T-cell-specific deletion in mice ($USP8^{f/f}$CD4-Cre) revealed that USP8 is essential for thymocyte transition to the $CD4^+$ and $CD8^+$ single positive stages and critical for TCR and Foxo1-mediated IL7Rα upregulation. *In vivo* reconstitution showed that enzymatic activity and SH3-binding are essential for USP8 function in T-cells. $USP8^{f/f}$CD4-Cre mice develop lethal colitis promoted by disturbed T-cell homeostasis, predominance of $CD8^+$ γδ-T-cells in the intestine and impaired regulatory T-cell function. Collectively, these data reveal an unexpected role of USP8 as an immunomodulatory DUB in T-cells.

Introduction

Ubiquitination plays a fundamental role in the immune system, but the physiological relevance of the more than 90 mammalian deubiquitinating enzymes (DUBs) is poorly defined[1, 2, 3, 4]. USP8 (synonym: UBPY) participates in endosomal sorting of transmembrane proteins[5, 6] and interacts with the SH3 domain of signal transducing adapter molecule 2 (STAM2), which is a component of the early acting endosomal sorting complex required for transport-0 (ESCRT-0)[7]. USP8 has been shown to deubiquitinate both cargo and ESCRT-0 proteins thus modulating their function and stability[5, 6]. Proteolytic cleavage of human USP8 was recently reported to increase its enzymatic activity and somatic mutations associated with increased processing were shown to cause Cushing´s disease by impairing EGFR downregulation[8].

USP8 contains two atypical SH3 binding motifs (SH3BMs) flanking a binding motif for 14-3-3 proteins (14-3-3BM), which were shown to inhibit USP8 activity[7, 8, 9, 10]. Peptide binding studies revealed that the N-terminal USP8 SH3BM binds even stronger to an SH3-domain of the GRB2-related adaptor downstream of Shc (GADS) than the C-terminal USP8 SH3BM binds to the STAM2 SH3-domain[11, 12]. GADS is predominantly expressed in T-cells and acts proximal to the T-cell receptor (TCR) to modulate signal diversification[13]. GADS forms a constitutive adaptor complex with the SH2 domain-containing leukocyte protein of 76 kDa (SLP76). Upon TCR activation GADS also associates with linker for activation of T-cells (LAT). However, it is unresolved, whether GADS interacts with USP8 *in vivo*. Furthermore, the function of USP8 in T-cells is entirely undefined.

In T-cells several ubiquitin E3 ligases like Casitas B-cell lymphoma-b (Cbl-b), ITCH, gene related to anergy in lymphocytes (GRAIL), and Roquin are essential for the induction of anergy. As a consequence, loss of these proteins is associated with autoimmunity[2, 14]. Likewise, several DUBs, like A20, USP9X, USP15, and Cylindromatosis (CYLD) were shown to be essential for proper T-cell function[1, 4, 15, 16]. Upon overexpression, USP8 was reported to form a complex with GRAIL and the DUB otubain1[17]. It was speculated that complex formation with an inactive isoform of otubain1 enables USP8 to deubiquitinate and stabilize GRAIL.

Besides TCR-mediated signals, T-cell function and development is controlled by cytokines and chemokines, which transmit signals through their cognate receptors. A tightly regulated key player in lymphocyte development and function is the interleukin-7 receptor (IL-7R), which is transiently downregulated on $CD4^+CD8^+$ double-positive (DP) thymocytes and re-expressed by $CD4^+$ and $CD8^+$ single positive (SP) thymocytes. In the periphery, it is highly expressed by naïve T-cells[18]. Forkhead box O1 (Foxo1) is a critical transcription factor positively controlling IL-7Rα expression[19, 20]. Foxo1 also directly or indirectly affects expression of Kruppel-like factor 2 (KLF2), CC-chemokine receptor 7 (CCR7) and CD62L[19,

[21]. In addition, Foxo1 controlled transcription programs were shown to be essential for regulatory T-cell (Treg) function[22]. Foxo1 itself is regulated by posttranslational modifications and sequestration by 14-3-3 proteins[23, 24].

Defects in TCR signaling or thymocyte development often cause chronic lymphopenia, which typically results in a proliferative response and conversion of T-cells from a naïve to an effector phenotype[21, 25]. IL-7R signaling and self-peptide-MHC complexes are vital for lymphopenia-induced proliferation and naïve T-cell homeostasis[21, 25]. Furthermore, altered T-cell homeostasis predisposes to the development of colitis typically promoted by defective Treg function[20, 26].

Here we show that USP8 represents a novel GADS and 14-3-3β-interacting protein that is processed upon TCR activation in a caspase-dependent manner. Furthermore, we provide evidence that USP8 is essential for normal T-cell development and homeostasis by securing maturation and Foxo1-mediated upregulation of IL7Rα. Concordantly, T-cell-specific inactivation of USP8 resulted in lethal colitis associated with dysfunction of Tregs towards highly abundant $CD8^+$ γδ T-cells in inflamed colons. These data establish USP8 as a novel DUB playing a key role in T-cell development and homeostasis.

Results

USP8 interacts with GADS and is proteolytically processed upon TCR stimulation

To identify potential USP8-interacting proteins in T-cells, a yeast two-hybrid (Y2H) screen was performed using fragments of USP8 as baits and a thymocyte-derived cDNA library. Bait 1 harboring the N-terminal SH3BM of USP8 yielded GADS as a binding partner. Furthermore, 14-3-3β was detected using bait 2, encompassing the 14-3-3BM of USP8 (**Supplementary Fig. 1**).

Interactions were confirmed in coimmunoprecipitation experiments with exogenously expressed, affinity-tagged proteins (**Fig. 1a and b**). To analyze the contribution of the USP8 SH3BMs to the interaction with GADS, critical proline residues were replaced by alanine (P405A, P738A and P405A/P738A). Replacement of the N-terminal proline (P405) significantly diminished USP8 binding to GADS (**Fig. 1a**)**.** The interaction with 14-3-3 proteins depends on phosphorylation of a serine within the binding motif. To evaluate the role of the USP8 14-3-3BM, the critical serine within this motif was replaced by alanine (S718A)[9]. Replacement of S718 abolished binding to 14-3-3β indicating that USP8 binds to 14-3-3β in a phospho-S718-dependent manner (**Fig. 1b**). Constitutive interaction of endogenous GADS and USP8 was confirmed in T-cells upon immunoprecipitation of endogenous USP8 (**Fig. 1c**)**.** Furthermore, endogenous 14-3-3β interacted with FLAG-tagged wild type (WT) USP8, but not USP8(S718A) (**Fig. 1d**)**.**

Individual TCRs are hypothesized to form nanoclusters in the absence of stimulation and to form microclusters upon activation[27]. As GADS and 14-3-3 proteins represent well-established proximal components of TCR signaling[13, 28], we asked whether USP8 might also participate. We therefore restimulated *ex vivo* grown $CD4^+$ T-cells with beads coupled to anti-CD3 and anti-CD28 antibodies, which trigger TCR- and costimulation simultaneously and allow the precipitation of TCR/CD28-associated proteins. USP8 and GADS were indeed identified to bind to the TCR/CD28 cluster and co-accumulate upon stimulation (**Fig. 1e**).

Intriguingly, upon TCR stimulation USP8 was proteolytically processed leading to the generation of an N-terminal 70 kDa cleavage product (**Fig. 1f**). USP8 cleavage was inhibited by pan-caspase inhibitor z-VAD pretreatment, indicating that USP8 is regulated in a caspase-dependent manner (**Fig. 1g**).

To evaluate whether GADS and 14-3-3β are modified by ubiquitin and might represent substrates for USP8-mediated deubiquitination, these proteins were coexpressed with WT USP8 or the USP8(C786A) variant lacking deubiquitinating activity. Consistent with ubiquitin modification, bands of higher molecular mass were detected for GADS and 14-3-3β upon coexpression and immunoprecipitation with USP8(C786A), but not WT USP8 (**Fig. 1h**). USP8-mediated modulation of GADS and 14-3-3β ubiquitination was confirmed by

coexpression of FLAG-tagged ubiquitin (**Supplementary Fig. 2a**). Furthermore, ubiquitination of 14-3-3β at lysines 9 and 189 was identified by mass spectrometry (**Supplementary Fig. 2b)**.

In summary, our results provide strong evidence that USP8 interacts with GADS and TCR signalosomes. We show that 14-3-3β interacts with USP8 via the 14-3-3BM in a serine phosphorylation-dependent manner. Our data suggest that GADS and 14-3-3β represent USP8 substrates, whereas USP8 is a target of caspase-dependent regulation.

USP8 is essential for T-cell development

To analyze the physiological role of USP8 in T-cells, USP8fl/fl mice [5] were mated to CD4Cre-transgenic mice. Deletion of USP8 in DP and $CD4^+$ SP (SP4) $USP8^{f/f}$CD4-Cre thymocytes was confirmed by Southern and/or Western blot (WB) analyses (**Fig. 2a, Supplementary Fig. 3a and 3b**). However, $CD8^+$ SP (SP8) thymocytes showed no reduction of USP8 expression (**Supplementary Fig. 3b**) presumably due to an advantage of escapees that reach an immature developmental stage without losing USP8 protein expression. Accordingly, $USP8^{f/f}$CD4-Cre mice exhibited significantly reduced percentages of SP4 and SP8 thymocytes resulting in a 2-3.5 fold decrease in total numbers, whereas total numbers of DP thymocytes were unaltered. Moreover, the reduction of SP8 thymocytes was even more pronounced within the TCR^{hi} subpopulation **(Fig. 2b)**. In agreement with a developmental defect in the transition from DP to SP thymocytes, medullary regions were sparsely distributed and smaller in thymi of $USP8^{f/f}$CD4-Cre mice **(Fig. 2c)**. Furthermore, the percentage of $CD25^+Foxp3^+$ Tregs among the $CD4^+$ cell population and the $NK1.1^+$ NKT-cell population were diminished **(Fig. 2d).** To characterize $CD4^-CD8^-$ double negative (DN), DP, SP4 and SP8 thymocytes, developmental markers were analyzed (**Fig. 2e**). TCRβ expression among SP4 and SP8 $USP8^{f/f}$CD4-Cre cells was diminished. While CD62L expression was reduced in SP4 cells, lower percentages of SP8 cells expressed CD5. CD24 downregulation, which also correlates with progressed maturation, was not observed in $USP8^{f/f}$CD4-Cre SP4 and SP8 cells. Higher percentages of $USP8^{f/f}$CD4-Cre SP4 cells strongly expressed CD69, indicating that more cells are engaged in early acting TCR-pMHC interactions[29]. Likewise, when $USP8^{f/f}LCK^{Cre}$ mice[30] were used, the USP8 protein depletion pattern was similar as in $USP8^{f/f}$CD4-Cre mice and did not reveal a defect in DN cell development (**Supplementary Fig. 3c and 3d**). However, a similar shift in SP4 and SP8 thymocyte populations and TCRβ expression as upon CD4Cre-mediated deletion was observed (**Supplementary Fig. 3e**). Taken together, these results show that USP8 is critical for thymocyte maturation.

USP8 is required for proliferation and IL-2 production, but not for negative selection of thymocytes

Ex vivo, lack of USP8 compromised thymocyte proliferation upon anti-CD3 stimulation in the absence or presence of IL-2 or anti-CD28 costimulation. Defects in proliferation were also observed when cells were stimulated with PMA/IONO, which bypasses proximal TCR signaling, indicating that lack of USP8 also affects downstream processes. Lack of proliferation was accompanied by diminished TCRβ expression (**Fig. 3a**). Differences in thymocyte apoptosis were not detected (**Supplementary Fig. 3f**). In addition, anti-CD3-stimulated USP8$^{f/f}$CD4-Cre thymocytes were unable to secrete IL-2 (**Fig. 3b**).

Qualitative alterations of T-cell signaling were previously shown to influence positive or negative selection within the thymus. For example, GADS knockout (KO) mice display defects in negative selection[31]. To analyze a potential role of USP8 in thymic selection, USP8$^{f/f}$CD4-Cre mice were crossed to HY-TCR transgenic mice expressing a transgenic TCR recognizing the male tissue-specific HY antigen. Similar to the situation in USP8$^{f/f}$CD4-Cre animals, percentages of mature SP4 or SP8 thymocytes were reduced in USP8$^{f/f}$CD4-CreHY-TCR^{+} female animals (**Fig. 3c**, upper panels). However, negative selection in male animals was not compromised in the absence of USP8 (**Fig. 3c**, lower panels).

Lack of USP8 impairs IL7Rα and CCR7 expression and Foxo1 activity

Unlike USP8-deficient mouse embryonic fibroblasts (MEFs) and hepatocytes[5], USP8$^{f/f}$CD4-Cre thymocytes did not display differences in the stability of STAM2 or overall ubiquitination compared to USP8$^{f/f}$ controls (**Supplementary Fig. 4a and b**). Moreover, endocytosis of the TCR upon stimulation was unaffected by the loss of USP8 (**Supplementary Fig. 4c**). These results suggest that the function of USP8 in T-cells differs from the previously described ESCRT-associated role in MEFs and hepatocytes. Furthermore, MAPK, Akt and IκB activation/phosphorylation, and IκB degradation in response to TCR stimulation, protein stability of 14-3-3β or GADS, NF-κB and activator protein 1 (AP-1) DNA-binding, overall tyrosine phosphorylation, and calcium influx were not altered in USP8$^{f/f}$CD4-Cre thymocytes (**Supplementary Fig. 4d-j**). These results suggest that USP8 is dispensable for canonical TCR signaling.

To detect primary alterations in USP8-deficient thymocytes, RNA expression profiles of DP thymocytes were analyzed by microarray analysis. Around 74 genes were dysregulated more than two-fold. Interestingly, IL7Rα mRNA showed the strongest downregulation in the absence of USP8 (**Supplementary Fig. 5a**). Ingenuity pathway analysis revealed a prominent network that centers around IL7Rα and Cyclin D2 expression (**Supplementary Fig. 5b**). Concordantly, upregulation of IL7Rα surface expression was impaired in USP8$^{f/f}$CD4-Cre SP thymocytes and IL7Rα mRNA expression levels were

decreased at the preceding DP stage of development (**Fig. 4a**). Similarly, CCR7 mRNA was found to be downregulated in USP8$^{f/f}$CD4-Cre DP thymocytes and CCR7 protein upregulation was blocked in SP4 thymocytes (**Fig. 4a**). However, a fraction of cells exhibited normal IL7Rα and CCR7 expression levels consistent with incomplete deletion (see Supplementary Fig. 3b). IL7Rα, CCR7 and CD62L (see Fig. 2e) constitute direct or indirect target genes of the transcription factor Foxo1, which is known to be regulated by 14-3-3 proteins[23, 24]. Thus, we speculated that the defect in expression of these genes might arise from a defect in Foxo1 stability or activity caused by the lack of USP8. Whereas Foxo1 protein levels and relocalization in response to TCR stimulation were unaltered in the absence of USP8 (**Fig. 4b** and data not shown), Chromatin immunoprecipitation (CHIP) analysis revealed that Foxo1 binding to the IL7Rα promoter is severely compromised in USP8$^{f/f}$CD4-Cre thymocytes (**Fig. 4c**). These results indicate that USP8 directly or indirectly affects thymocyte development via the Foxo1-IL7R axis.

USP8 is critical for T-cell homeostasis

Consistent with the defect in thymocyte development, the percentages of SP4 and SP8 T-cells and total T-cell numbers in spleen and mesenteric lymph nodes (MLNs) of USP8$^{f/f}$CD4-Cre mice were strongly reduced (**Fig. 5a, Supplementary Fig. 6a** and data not shown). Southern blot analysis revealed that USP8 gene deletion in peripheral T-cells is incomplete indicating that cells which failed to delete USP8 have an advantage in the periphery (**Supplementary Fig. 6b**). Naïve CD4$^+$ T-cells were strongly reduced in the periphery of USP8$^{f/f}$CD4-Cre mice and the percentages of CD44^{hi} effector (CD62L^{lo}) and memory (CD62L^{hi}) T-cells were elevated **(Fig. 5a)**. Remaining effector T-cells were identified to represent escapees of USP8 deletion (**Supplementary Fig. 6c**). IL-7Rα expression was reduced in the few remaining naïve T-cells, but not in effector T-cells (**Supplementary Fig. 6d**). LCKCre-mediated deletion of USP8 also caused a severe reduction of the percentages of T-cells in the periphery, pronounced diminishment of the naïve T-cell population and a decrease in IL-7Rα expression on naïve T-cells (**Supplementary Fig. 6e**).

CCR7 expressing CD4$^+$ cells were also almost absent in the periphery of USP8$^{f/f}$CD4-Cre mice (**Supplementary Fig. 6f**). In spleen, no significant differences in the percentages of Tregs (relative to the CD4$^+$ population), granulocytes, monocytes, plasmacytoid dendritic cells (pDCs), or conventional DCs (relative to CD3$^-$ populations) were observed (**Fig. 5b**). The percentages of Tregs relative to the CD4$^+$ population and of pDCs were significantly increased in MLNs (**Fig. 5c**). However, due to the decrease in overall T-cell numbers also total numbers of Tregs were reduced. A higher percentage of CD4$^+$ USP8$^{f/f}$CD4-Cre splenocytes produced interferon γ (IFNγ) and IL-17 after PMA/IONO stimulation (**Fig. 5d**). Moreover, percentages of cells expressing the activation markers CD25 and CD69 were

increased among peripheral USP8$^{f/f}$CD4-Cre CD4^{+} T-cells. Concordantly, expression of the negative activation markers CD45RB and TCRβ was diminished in spleen and expression of TCRβ was reduced in MLNs (**Fig. 5e**). These results show that USP8 is critical for T-cell homeostasis *in vivo.*

CD4Cre-mediated deletion of USP8 causes lethal colitis

Intriguingly, USP8$^{f/f}$CD4-Cre mice spontaneously developed colitis. Pathological and endoscopic analysis revealed colon thickening and inflammation emanating from the distal part of the colon resulting in enhanced granularity, loss of the vascular pattern of the mucosa and a reduction in translucency. Frequently, intestinal prolapses were observed. Colitis was typically accompanied by lymphadenopathy and splenomegaly (**Fig. 6a and movies S1/S2**). Starting from week 6, animals became moribund and died within 20 weeks with almost 100% penetrance (**Fig. 6b**). Histological analysis showed thickening of the mucosa, cryptic abscesses, cellular infiltrates, epithelial hyperplasia and elongated crypts **(Figure 6c,** upper left panels). Intriguingly, among infiltrating cells a large portion were CD3^{+} T-cells. Foxp3^{+} Tregs were also detected **(Figure 6c,** lower left panels). Massive infiltrates of DCs, neutrophils and macrophages were present in inflamed colon sections of USP8$^{f/f}$CD4-Cre mice (**Fig. 6c**, right panels). Splenomegaly was characterized by a reduced size of the periarteriolar lymphoid sheaths and concomitant enlargement of the Ki-67 positive red pulp compartment containing Mac-3^{+} myeloid cells (**Fig. 6d**).

USP8 is an intrinsic regulator of T-cell development and homeostasis

To analyze the function of USP8 in mature T-cells irrespective of phenotypes through modified thymocyte development, we crossed USP8$^{f/f}$ animals to transgenic mice expressing tamoxifen-inducible Cre specifically in CD4^{+} T-cells (USP8$^{f/f}$CD4-CreER^{T2})[32]. To restrict USP8 deletion to peripheral T-cells, RAG2/Il2rg double deficient mice were reconstituted with splenocytes derived from USP8$^{+/+}$CD4-CreER^{T2} or USP8$^{f/f}$CD4-CreER^{T2} mice. Tamoxifen-induced deletion of USP8 caused a significant reduction of CD4^{+} splenocytes and CD44^{lo}CD62L^{hi} CD4^{+} T-cells, demonstrating that USP8 is essential for the maintenance of the naïve CD4^{+} T-cell pool (**Fig. 7a**). To test whether USP8-deficient T-cells have an intrinsic defect in thymocyte development and peripheral T-cell homeostasis, or whether the defect(s) can be overcome by the presence of WT T-cells, we generated CD45.1^{+}WT/CD45.2^{+}USP8$^{f/f}$ and CD45.1^{+}WT/CD45.2^{+}USP8$^{f/f}$CD4-Cre BM chimeras. Even in the presence of WT thymocytes and peripheral T-cells, CD45.2^{+}USP8$^{f/f}$CD4-Cre T-cells exhibited a defect in thymocyte development and expansion/survival in the periphery accompanied by a shift towards effector/memory populations (**Fig. 7b**). This shift was less severe than in USP8$^{f/f}$CD4-Cre mice (% naive CD4^{+}CD44^{lo}CD62L^{hi} T-cells: 15.45±3.95 versus 3.22±0.83,

p<0.01, unpaired, 2-sided t-test) (see also Fig. 5a), indicating that the effect partially depends on lymphopenia-induced homeostatic expansion most likely caused by escapees of USP8 deletion. In addition, more peripheral USP8$^{f/f}$CD4-Cre T-cells produced IFNγ and IL-17 upon PMA/IONO treatment. Altogether, these findings demonstrate that USP8 is an intrinsic regulator of both thymocyte development and peripheral T-cell homeostasis.

Likewise, we investigated whether reduced IL7-R expression is a cell intrinsic consequence of the USP8 defect. IL7Rα surface expression was impaired in CD45.2^{+} USP8$^{f/f}$CD4-Cre SP thymocytes suggesting that here USP8 depletion directly affects IL7Rα expression. In peripheral CD45.2^{+} USP8$^{f/f}$CD4-Cre naïve T-cells of competitive BM chimeras, IL7Rα expression was not decreased. Therefore, reduced IL-7Rα expression on naïve T-cells as seen in the non-competitive background appears to be caused by extrinsic mechanisms. Homeostatic expansion of cells which failed to delete USP8 probably accounts for this effect (**Supplementary Fig. 6g**).

USP8 is dispensable for canonical TCR signaling in peripheral T-cells

As the dramatic reduction of the naïve T-cell population in USP8$^{f/f}$CD4-Cre mice hampered further analysis, we took advantage of the 4-hydroxytamoxifen (OHT)-inducible CreER^{T2} system to analyze signaling in T-cells upon deletion of USP8 before manifestation of secondary effects on cell proliferation and CD3 expression. We found maximum suppression of USP8 protein expression in cultured USP8$^{f/f}$CD4-CreER^{T2} CD4^{+} T-cells 48h post OHT addition (**Fig. 7c**, upper panels), whereas a reduction of CD3 and Ki67 expression became apparent starting at 72h post OHT addition (**Fig. 7c**, lower panels). We therefore restimulated CD4^{+} T-cells 48h after OHT treatment with anti-CD3/anti-CD28 antibodies and monitored phosphorylation/activation state and expression of an array of signaling molecules. LAT and PLCγ phosphorylation was high in unstimulated cells of both genotypes and was downregulated upon restimulation, which correlated with normal ERK1/2 activation (**Supplementary Fig. 7a**). Moreover, GADS and 14-3-3β expression, IκB, p38 and PKB phosphorylation, global K48-linked ubiquitination, tyrosine-, SLP76(S376)- and JNK-phosphorylation, and Foxo1 and GRAIL protein levels were unaltered (**Supplementary Fig. 7b-d**). Because USP8 was shown to regulate endosomal trafficking, we next asked whether the protein is involved in proper assembly of the TCR signalosome upon activation, which has been hypothesized to involve the recruitment of subcellular LAT-containing vesicles[13]. In agreement with normal LAT phosphorylation, recruitment of signaling molecules including 14-3-3β correlated with the amount of CD3 in the purified complexes (**Supplementary Fig. 8a**). Furthermore, the amount of the overall complex purified upon TCR stimulation did not differ significantly in four independent experiments. In summary, these data strongly suggest that similar to thymocytes USP8 is dispensable for canonical CD3/CD28-induced receptor-

proximal signaling in mature T-cells. As shown in Jurkat-derived KO cell lines, lack of SLP76 did not influence USP8 co-accumulation with the TCR/CD28 cluster, whereas LAT was crucial for signalosome formation. However, USP8 binding was not abolished in the absence of GADS (**Supplementary Fig. 8b**) suggesting that other interaction partners or motifs of USP8 contribute to the binding to the signalosome. Furthermore, our results show that USP8 also interacts with the TCR/CD28 cluster in human cells.

Catalytic activity and SH3 binding capacity are crucial for the function of USP8 in T-cells

To gain mechanistic insight into structure-function relationships of USP8 in T-cells, we used an *in vivo* rescue approach. To this end, USP8$^{f/f}$CD4-Cre BM stem cells were reconstituted with retroviruses ectopically expressing EGFP in combination with either WT USP8 or variants lacking either catalytic activity (C748A), SH3 binding capacity (P405/700A) or the phosphorylation site required for 14-3-3 binding (S680A). Subsequently, these cells were transplanted into lethally irradiated RAG1-deficient recipients and the distribution of splenic T-cell subsets was analyzed 8 weeks later. Reconstitution with either an empty vector or the USP8 variant lacking isopeptidase activity entirely failed to rescue T-cell development (**Fig. 7d**). Likewise the USP8 variant which lacks the SH3BMs and can no longer interact with GADS (see Fig. 1a) failed to restore the T-cell compartment. In contrast, cells expressing WT USP8 entirely restored the T-cell compartment and also the 14-3-3 binding mutant did not show significant defects in rescue capability (**Fig. 7d**).

These results clearly show that both catalytic activity of USP8 and the SH3BMs but not 14-3-3 binding, are essential for USP8 function in T-cells.

USP8 is necessary for Treg function against proinflammatory γδ T-cells

The intraepithelial lymphocyte (IEL) population of the gut represents the environmental interface with the highest abundance of mostly CD8$^+$ TCRγδ$^+$ T-cells[33]. IEL TCRγδ$^+$ T-cells have been described previously to be responsible for intestinal inflammation in mice lacking phosphoinositide-dependent protein kinase 1 (PDK1) in T-cells[26]. PDK1 acts downstream of PI3K and is also crucial for the maintenance of functional Tregs. Because our histological analysis revealed disproportional high recruitment of CD3$^+$ T-cells to inflamed colons of lymphopenic USP8$^{f/f}$CD4-Cre mice, we examined whether these cells are TCRαβ- or TCRγδ-positive. Indeed, our results show that CD8$^+$TCRγδ$^+$ T-cells are the main T-cell population among USP8$^{f/f}$CD4-Cre IELs in inflamed colons (**Fig. 8a**). In contrast to USP8$^{f/f}$CD4-Cre TCRαβ$^+$ T-cells, surface expression of the activation marker CD69 was not compromised in TCRγδ$^+$ T-cells (**Fig. 8a**). Elevated percentages of CD8$^+$ TCRγδ$^+$ T-cells were also found in MLNs of USP8$^{f/f}$CD4-Cre mice (**Fig. 8b**). More USP8$^{f/f}$CD4-Cre TCRαβ$^+$ T-

cells expressed CD69 in MLNs, which is consistent with the data shown in Fig. 5e. We found that the numbers of γδ T-cells were 8-10-fold higher in MLNs of both, USP8$^{f/f}$CD4-Cre (**Fig. 8c**) and USP8$^{f/f}$LCK^{Cre} mice (data not shown), and 4-fold in the USP8$^{f/f}$CD4-Cre T-cell population of mixed BM chimaera (**Fig. 8c**). Furthermore, quantification of blood cytokine levels revealed that the pro-inflammatory cytokines IL-6 and IL-12p70 were significantly elevated in the serum of diseased USP8$^{f/f}$CD4-Cre mice. Elevated levels of IFNγ and TNFα were also detected in these mice, whereas upregulation of IL-10 and IL-17 was not observed (**Fig. 8d** and data not shown). To examine whether USP8 is crucial for the functional capacity of Tregs, we performed an *in vivo* Treg assay. Our results demonstrate that co-injection of USP8$^{f/f}$CD4-Cre Tregs does not prevent the onset of colitis in Rag1-/- mice that were reconstituted with naïve CD4^{+} WT cells (**Fig. 8e**). USP8-deficient Treg cells were also less effective than control Treg cells in inhibiting naïve T-cell proliferation *in vitro* (**Fig. 8f**). For Treg-specific Foxo1 KO cells it has been shown that lack of function is caused by a deregulated IFNγ response[22]. Likewise, we observed an increased IFNγ response in USP8 depleted Tregs (**Fig. 8g**). These data demonstrate that USP8 is required for the maintenance of enteric immune tolerance by Treg cells via suppression of an inflammatory response mediated by intestinal γδ T-cells.

Discussion

Here we show that the DUB USP8 is a previously unidentified component of the TCR signaling complex interacting with GADS and 14-3-3β. Previous studies have shown that a peptide comprising the conserved C-terminal SH3BM in USP8 binds the STAM2-SH3[12]. Intriguingly, a peptide derived from one of the two GADS-SH3 domains binds to the N-terminal USP8 SH3BM with more than 25fold higher affinity[11]. This is consistent with our observation that GADS was detected in our Y2H screen by the bait encompassing the N-terminal SH3BM of USP8. As GADS expression is largely restricted to lymphocytes, high affinity binding to GADS might explain why, in contrast to MEFs and hepatocytes, STAM2 stability and endosomal sorting appear unaffected in USP8-depleted T-cells[5]. Ectopic re-expression of an USP8 mutant lacking the SH3BMs did not rescue T-cell development. This clearly shows that the SH3BM-mediated interactions are essential for the function of USP8 in T-cells and suggests that USP8/GADS-binding mediated by the atypical N-terminal SH3BM in USP8 is critical for the specificity of USP8 function in T-cells[7, 11, 12]. Our *in vivo* rescue experiments also demonstrate that the catalytic activity is essential for USP8 function in T-cell development. This is of particular interest as different DUBs such as A20 or USP18 were shown to possess physiologically relevant non enzymatic functions[34, 35, 36].

Within this study we identified 14-3-3β as a binding partner of USP8. As typical for 14-3-3 proteins, this interaction was dependent on a serine phosphorylation motif within the 14-3-3BM of USP8[23]. 14-3-3ε, λ, and ζ binding to USP8 was previously shown to exert an inhibitory effect on USP8 catalytic activity[8, 9]. Thus, serine phosphorylation-dependent binding of 14-3-3β might negatively regulate USP8 catalytic function in T-cells. Remarkably, upon TCR-stimulation USP8 gets cleaved by a caspase-dependent mechanism. Consistent with the resulting N-terminal 70kDa cleavage product observed in our study, a recent report showed that human USP8 mutants undergo proteolytic cleavage within the 14-3-3 binding region resulting in enhanced DUB activity[8]. Thus, it is well conceivable that 14-3-3β binding and proteolytic processing contrarily regulate USP8 DUB activity in a TCR stimulation dependent manner.

Our findings strongly suggest that GADS and 14-3-3β represent substrates for USP8-mediated deubiquitination. Unaltered stability in the absence of USP8 and a modification pattern typical for mono-ubiquitination indicates that USP8-mediated deubiquitination of GADS and 14-3-3 regulates protein complex composition rather than stability of these proteins. Interestingly, for both SLP76 and GADS, TCR-induced interactions with 14-3-3 proteins have been described with the functional consequence of a negative feedback inhibition of TCR signaling and uncoupling from LAT[28, 37].

USP8 has previously been suspected to regulate the stability of GRAIL [38]. However, we did not detect any differences in GRAIL stability in the absence of USP8.

CD4Cre- as well as LCKCre-mediated USP8 deletion caused a defect in SP thymocyte maturation. During SP thymocyte development, low-affinity TCR interactions with self-peptide-MHC trigger a signaling cascade that allows for positive selection[13]. Although our studies did not reveal any differences in negative selection or TCR-induced canonical signaling cascades, we cannot exclude that USP8 is involved in the discrimination of low- and high-affinity signals in specific cell populations. Likewise, USP8 may control TCR-stabilization and upregulation during development. Thus, USP8 may indirectly influence thymocyte maturation and IL-7Rα upregulation. According to the kinetic signaling model of T-cell development, cytokine receptor signals specify the lineage fate of MHC-I-selected thymocytes, whereas TCR signals specify the lineage fate of MHC-II-selected thymocytes[39]. Similar to T-cell-specific IL7R KO mice, USP8$^{f/f}$CD4-Cre animals showed a marked reduction of SP8 cells among TCRβ^{hi} thymocytes. However, the defect in SP4 maturation suggests that IL7R-independent mechanisms are affected as well.

Our data indicate that USP8 is critical for Foxo1 activity in thymocytes. USP8 regulation of 14-3-3β ubiquitination may directly affect the potential of 14-3-3β to regulate Foxo1 DNA binding in the nucleus similar to what has been shown for the regulation of DAF-16 and Foxo4 by 14-3-3 proteins[23]. High nuclear activity of Foxo1 was shown to be essential for Treg activity. Importantly, Foxo1 controls the expression of Foxp3 and a subset of Treg-associated genes and is critical for the suppression of IFNγ expression, which is also compromised in USP8-deficient Tregs[22, 40]. Thus, impaired Foxo1 activity as detected in USP8-deficient thymocytes might provide an explanation for the compromised Treg function observed in USP8$^{f/f}$CD4-Cre mice. Accordingly, in a bone marrow (BM) transfer model using sublethally irradiated Rag1-/- mice, lack of Foxo1 expression in T-cells resulted in colitis presumably due to defective Treg abundance and function[20]. Consistent with the gut representing the interface with the highest abundance of γδ T-cells, colitis in USP8$^{f/f}$CD4-Cre mice was associated with a dysfunction of regulatory T-cells towards highly abundant CD8^{+} γδ T-cells in inflamed colons. γδ T-cells have already been shown to play an exacerbating role in chronic colitis in TCRα mutant mice and PDK1$^{f/f}$CD4-Cre mice[26, 41].

In accordance with the phenotype displayed by T-cell-specific USP8 KO mice, T-cell-specific deletion of the Foxo1 gene in mice led to defects in IL-7–dependent homeostatic proliferation *in vivo* as well as spontaneous T-cell activation and effector T-cell differentiation[20, 42]. In addition to defective Foxo1 regulation, the failure in IL-2 secretion and CCR7 upregulation in thymocytes and the observed lack of IL-10 up-regulation in diseased USP8$^{f/f}$CD4-Cre mice could per se account for defective *in vivo* Treg function and/or susceptibility to colitis[43, 44, 45].

In conclusion, we have identified USP8 as a GADS-interacting DUB associated with the TCR signalosome. The previously undefined role of USP8 in T-cell development, immune

446 homeostasis and control of Foxo1 target gene expression may provide new avenues for the
447 treatment of immunological disorders.
448

Methods

Methods and any associated references are available in the online version of the paper.

Note: Any Supplementary Information and Source Data files are available in the online version of the paper.

Acknowledgements

We thank M. Oberle, C. Fix, T. el Gaz, A. Nikolaev, and T. Bass for excellent technical assistance, J. Wersing for cell sorting, S. Hemmers for support with generation of the CD4CreER^{T2}-transgenic mice, A. Izcue for protocols, and S. Feller and E. Martegani for USP8 antibodies. This work was supported by grants of the Deutsche Forschungsgemeinschaft to K.P.K. (KN590/4-1) and to W.W.S. through EXC294 (the Center for Biological Signaling Studies, *BIOSS*).

Author Contributions

A.D. designed and performed experiments, analyzed the data and wrote the paper; A.K. designed and performed experiments; S.N. generated the conditional USP8 KO mice and designed and performed experiments. A.B. performed the Y2H screen; A.W. and S.R. contributed to or carried out the endoscopic recording and histological analyses; A.S. provided help with experiments; M.G. and A.A. contributed to the Y2H screen and provided reagents. T.K. performed the gene expression microarray analysis; A.S. performed mass spectrometric identification of ubiquitination sites; T.B. generated CD4CreER^{T2}-transgenic mice; W.W.S. provided reagents and contributed to the calcium influx experiment; M.P. contributed to the histological analyses. K.-P.K. supervised the project and wrote the paper.

Competing Financial Interests

The authors declare no competing financial interests.

Material and Methods

Mice.

USP8$^{f/f}$, RAG2/Il2rg double KO, CD4Cre-, CD4CreER^{T2}-, LCKCre-, and HY-TCR transgenic mice have been described previously[5, 30, 32, 46, 47, 48]. Mice used for experiments were on the C57BL/6 background. Histological examinations of the colon and the survival studies with USP8$^{f/f}$CD4-Cre mice were done on mixed C57BL/6-129OLA background. If not otherwise stated, 8-week to 3-month old, sex-matched littermates were used in all experiments. The survival study was performed with age- and sex-matched mice for the indicated observation period. Animals were housed in a specific pathogen-free barrier facility according to the protocols of the Center for Experimental Models and Transgenic Services (CEMT) at the University Clinic in Freiburg. All experiments were approved by national authorities (G-10/101) and the ethics review board for animal studies at the University of Freiburg.

Southern blotting and real-time PCR.

WT, loxP-flanked and deleted USP8 alleles were identified by Southern blotting of NcoI fragments of genomic DNA as described before[5]. For real-time PCR, DP thymocytes were isolated by cell sorting and RNA was isolated using the RNeasy Mini Kit (Qiagen) following the manufacturer's instructions. Samples were treated with DNaseI (Roche) and RNA was transcribed into cDNA using oligo-dT primers and the SuperScript II RT kit (Invitrogen). RT-PCR reactions were performed using LightCycler 480 SYBR Green I master mix (Roche) and the following primers: IL7Ra_S: TGGGGCTCTTTTACGAGTGA; IL7Ra_AS: TTGCTTCTTTGCGATAAACG; CCR7_S: TGATTTCTACAGCCCCCAGA; CCR7_AS: GCACACCTGGAAAATGACAA; Cyclin D2_S: GCGTGCAGAAGGACATCCA; Cyclin D2_AS: CACTTTTGTTCCTCACAGACCTCTAG; GAPDH_S: TCCTGCACCACCAACTGCTTAGCC; GAPDH_AS: GTTCAGCTCTGGGATGACCTTGCC.

Cell preparation and flow cytometry.

Thymi, spleens and MLNs were mashed into single-cell suspensions in PBS containing 1 % FCS and splenocytes were depleted of red blood cells using RBC lysis buffer (Sigma). Cell suspensions were incubated with mouse BD Fc Block™. CD4$^+$ T-cells were enriched by the use of the mouse CD4 T lymphocyte enrichment set – DM from BD Biosciences or purified using BD IMag™ anti-mouse CD4 particles-DM (BD Biosciences). DP thymocytes were enriched using BD IMag™ anti-mouse CD8a particles-DM (BD Biosciences). BM from tibias and femurs was obtained by flushing with PBS containing 1 % FCS and depleted of red blood cells using RBC lysis buffer (Sigma). Stimulation of IFNY and IL-17 producing cells was performed in RPMI media (RPMI-1640 media containing penicillin/streptomycin, 50 µM

β-mercaptoethanol and 10 % FCS) with 50 ng/ml PMA and 1 µg/ml Ionomycin (Sigma) for 4 h in the presence of GolgiPlug (BD Biosciences). IELs were prepared as described previously[26]. For FACS analysis cells were stained with antibodies (Abs) from BD Pharmingen directed against CD4 (RM4-5), CD8a (53-6.7), TCRβ (H57-597), CD24 (M1/69), CD5 (53-7.3), CD25 (PC61), Foxp3 (MF23), Ki67 (B56), IL-7Rα (A7R34), CD44 (IM7), CD62L (MEL-14), B220 (RA3-6B2), IFNγ (XMG1.2), IL-17A (TC11-18H10), CD45RB (16A), CD45.1 (A20), CD45.2 (104), CD69 (H1.2F3), and Ly6C (AL-21) and with Abs from eBioscience directed against NK1.1 (PK136), CD3e (500A2), CCR7 (4B12), CD11b (M1/70), αβTCR specific for the H-Y antigen (T3.70), Foxp3 (FJK-16s), MHCII (M5/114.15.2), Ly6G (RB6-8C5), CD115 (AFS98), CD11c (N418), and γδ TCR (UC7-13D5). Intracellular Foxp3 was stained using the BD Pharmingen mouse Foxp3 buffer set or the eBioscience Foxp3 staining buffer set, intracellular IL-17 and IFNY using the eBioscience Foxp3 staining buffer set. Expression of surface and intracellular markers was analyzed using a flow cytometer (BD FACSCanto™ II) and FlowJo software.

T-cell stimulation, expansion and apoptosis.

Freshly isolated thymocytes were prepared as described above and plated at $1x10^6$ cells/ml in round-bottom 96-well plates in RPMI media. Thymocytes were stimulated with plate-bound anti-mouse CD3e (145-2C11) and 2 µg/ml anti-mouse CD28 (37.51) from eBioscience, 100 U/ml recombinant murine IL-2 (ImmunoTools), or 10 ng/ml PMA and 100 ng/ml Ionomycin as indicated. Apoptosis was determined using the FITC Annexin V apoptosis detection kit from BD Pharmingen™. Proliferation was assessed using the PE mouse anti-human Ki-67 set from BD Pharmingen™. For peripheral T-cell expansion, $CD4^+$ T-cells from spleen were enriched as described above and cultured for 48 h in RPMI-1640 media with 10 % FCS on 6-well plates coated with anti-hamster IgG_1 (clone G94-56, BD Pharmingen) in the presence of soluble anti-mouse CD3e (1 µg/ml) and anti-mouse CD28 (1 µg/ml). Subsequently, cells were diluted into medium containing IL-2 at a concentration of 100 U/ml. If the cells were treated with 4-hydroxytamoxifen (OHT, Sigma), OHT was added to a final concentration of 1 µM. For the stimulation and preparation of protein lysates, thymocytes or $CD4^+$ T-cells were starved in RPMI-1640 media without FCS for 2 h and activated by preincubation with soluble anti-mouse CD3ε (10 µg/ml) and anti-mouse CD28 (2 µg/ml) on ice for 30 min followed by stimulation at 37ºC with prewarmed anti-hamster IgG_1 (5 µg/ml, BD Pharmingen) for the times indicated. Z-Vad (R&D Systems) was used at a final concentration of 40 µM.

Cell lines, expression constructs and transfection.

Jurkat-derived GADS-deficient cells were described recently[49]. USP8, GADS and 14-3-3β expression constructs were generated from human cDNA. C-terminally FLAG-tagged USP8 was expressed using the pFLAG-CMV5α vector; C-terminally HA-tagged 14-3-3β and N-terminally HA-tagged GADS using pcDNA3.1 vectors. Retroviral expression vectors for N-terminally E-tagged (ETAG-)USP8 were generated from mouse cDNA using MIEG3 vector. Retroviral particles were produced in Platinum-E retroviral packaging cells according to standard protocols. Point mutations were generated by site-directed mutagenesis using the QuikChange® mutagenesis system (Stratagene). The Flag-ubiquitin-pCAGGS vector was a kind gift from the laboratory of Rudi Beyaert, Ghent University. HEK293T-cells were transfected using FuGENE HD Transfection Reagent from Roche and harvested 36 h post transfection.

Western blotting, TCR signalosome purification and immunoprecipitation.

Lymphocytes, thymocytes and HEK293T cells were lysed in *n*-Dodecyl-β-D-maltoside (DDM) lysis buffer (50 mM Tris-HCl, pH 7,4; 150 mM NaCl; 1 mM EDTA; 50 mM NaF; 1 mM sodium vanadate; 1x Roche complete protease inhibitor cocktail; 0.2% DDM). Immunoprecipitations (IPs) were performed using anti-FLAG M2 affinity gel from Sigma or rat monoclonal anti-HA antibody (Ab) (clone 3F10) affinity matrix from Roche. Direct IP was performed using the Pierce® Direct IP kit according to the manufacturer's protocol. The TCR signalosome was purified as described before[50], except for the additional use of Dynabeads® Mouse T-activator CD3/CD28 beads (Lifetechnologies) and the replacement of 600 mM KCl with 600 mM NaCl during the last two washing steps with "freeze-thaw" buffer. WB analysis was performed with Abs from Santa Cruz Biotechnology directed against GADS (UW40, 73652), STAM2 (F-11, 365600), 14-3-3β (H-8, 1657), CD3ε (M20, 1127), PLCγ_1 (1F1, 58407), SLP76 (H300, 9062), and Actin (I19, 1616); with Abs from Sigma directed against tubulin (clone 2-28-33, T5293) and Flag (M2); with Abs from Cell Signaling Technology directed against phospho-p44/42 (197G2, 4377), phospho-JNK (81E11, 4668), phospho-p38 (3D7, 9215), phospho-AKT (9271), phospho-IκBα (14D4, 2859), IκBα (9242), FoxO1 (C29H4, 2880), SLP76 (4958), phospho-SLP76 (S376, 13177), phospho-LAT (Y191, 3584), phospho-PLCγ (Y783, 2821), K48-linkage specific polyubiquitin (D9D5, 8081), and K63-linkage specific polyubiquitin (D7A11, 5621); with Abs from abcam directed against Themis (101038) and the E-tag (10B11, ab3397); with peroxidase-coupled anti-HA Ab (3F10, Roche), anti-LAT Ab (06-807, Millipore), anti-phosphotyrosine Ab (PY20, BD Biosciences, 610000) or peroxidase-coupled anti-phosphotyrosine Ab (4G10, Millipore), and anti-GRAIL Ab (synonym: RNF128, EPR7426(2), abcam 137088). The peptide affinity-purified polyclonal USP8 Ab raised

against amino acids (aa) 19-32 of mouse USP8 was kindly provided by Dr. Stephan Feller, University Clinic Halle (Saale). The X39 Ab raised against aa 542-660 of mouse USP8 was kindly provided by Dr. Enzo Martegani, University of Milano-Bicocca. Densitometric analysis was performed using ImageJ software.

Ca^{2+} influx.

DP thymocytes were enriched as described above. Thymocytes were starved and loaded with indo-1-AM (5 µg/ml) for 30 min at 37ºC in RPMI-1640 media without FCS. Subsequently, thymocytes were incubated with soluble anti-mouse CD3e (10 µg/ml) and anti-mouse CD28 (2 µg/ml) in RPMI-1640 media containing 10% FCS on ice for 20 min and stimulated at 37ºC with pre-warmed anti-hamster IgG. The emission wavelength ratios of intracellular Ca^{2+}-bound and -unbound indo-1-AM were analyzed on a LSR II flow cytometer using FACS Diva software (BD Biosciences).

Preparation of nuclear extracts and EMSA.

Nuclear extracts were harvested as described previously[51]. The EMSA was performed using the Odyssey Infrared EMSA kit and NF-κB and AP-1 probes from LI-COR.

ChIP assay.

Chromatin IP (ChIP) assays were done using the Millipore ChIP Assay kit according to the manufacturer's instructions. $CD4^+$ thymocytes were isolated using BD IMag™ anti-mouse CD4 magnetic particles-DM (BD Biosciences). Sonication of fixed and lysed cells was performed using a Branson sonifier cell disruptor B15 (output intensity: 4; 10 x 12 pulses at 90% duty cycle). IP was performed using anti-FKHR Ab (H128, Santa Cruz) or rabbit IgG (control)[19]. PCR (T_m= 62ºC; 35 cycles) was performed with the Il7ra-ECR2 S and Il7ra-ECR2 AS primers reported previously[19].

ELISA and Luminex assay.

IL-17 serum concentrations were determined using the mouse IL-17 DuoSet ELISA kit (R&D Systems); mouse IL-10 concentrations using the Quantikine ELISA kit (R&D Systems). IFNγ, TNFα, IL-6, IL-12p70, IL-4 and IL-5 serum levels were quantified using the ProcartaPlex™ Mouse Th1/Th2 essential 6plex Immunoassay (eBioscience).

Histology.

H&E and immune histological staining of colonic sections with Abs directed against CD3 and Foxp3 were carried out as described previously[52]. Immunofluorescence of cryo-sections was performed using the TSA Cy3 system (PerkinElmer), a fluorescence microscope (IX70;

Olympus) and primary Abs against CD11c (HL3, BD Biosciences), MPO (15484, Abcam), and F4/80 (BM8, eBioscience). In brief, cryo-sections were fixed in ice-cold acetone for 10 minutes followed by sequential incubation with methanol, avidin/biotin (Vector Laboratories), and protein blocking reagent (Dako). Slides were then incubated overnight with primary Abs. Subsequently, the slides were incubated for 30 minutes at room temperature (RT) with biotinylated secondary Abs (Dianova). All samples were finally treated with streptavidin-horseradish peroxidase and stained with tyramide (Cy3) according to the manufacturer's instructions (Perkin Elmer). Before examination, nuclei were counterstained with Hoechst 3342 (Invitrogen). Histological staining of splenic and thymic paraffin sections were carried out using Abs directed against CD3 (1:100, Serotec, MCA1477), B220 (1:200, BD Pharmingen 557390), MAC-3 (1:200, BD Pharmingen 553322), and Ki67 (1:50, DAKO M7249).

Endoscopy.

For *in vivo* mini-endoscopy analysis of colons, a high-resolution video endoscopic system (Karl Storz) was used. To determine colitis activity, mice were anesthetized by injecting a mixture of ketamine (Ketavest 100 mg/ml, Pfizer) and xylazine (Rompun 2%, Bayer Healthcare) i.p. and monitored by mini-endoscopy. Endoscopic scoring of five parameters (translucency, granularity, fibrin, vascularity and stool) was performed.

***In vitro* and *in vivo* Treg assay.**

For the preparation of $CD4^+CD45RB^{hi}CD25^-$ naïve and $CD4^+CD45RB^{lo}CD25^+$ regulatory T-cells, cell suspensions were prepared from spleens and MLNs and $CD4^+$ T-cells were enriched as described above and stained. Naïve T-cells and Tregs were isolated by cell sorting. $5x10^4$ $USP8^{f/f}$ $CD4^+CD45RB^{hi}CD25^-$ responding T-cells (Tresp) were labeled with CFSE and cultured with $CD4^+CD45RB^{lo}CD25^+$ $USP8^{f/f}$ or $USP8^{f/f}$CD4-Cre Treg cells at a ratio 1:1, or without Treg cells for 72 h after stimulation with anti-CD3 Ab (2 µg/ml) in the presence of $1x10^5$ irradiated splenocytes (30 Gy). The division of Tresp cells was assessed by dilution of CFSE (Molecular Probes™).

For the analysis of *in vivo* Treg function, Rag1-/- mice were intraperitoneally injected with $4x10^5$ $USP^{f/f}$ naïve T-cells in the absence or presence of $1x10^5$ $USP8^{f/f}$ (WT) or $USP8^{f/f}$CD4-Cre (KO) Tregs. Mice were analyzed 9 weeks post injection.

Generation of BM chimera.

$CD45.1^+$ mice were irradiated with a dose of 7 Gy and cotrimoxazol was added to the drinking water. The next day BM was prepared from donor mice as described above and

mice were intravenously injected with 5-10 x 10^6 cells (1:2 mixture of BM from CD45.1$^+$ and CD45.2$^+$USP8$^{f/f}$ or CD45.2$^+$USP8$^{f/f}$CD4-Cre mice). The reconstituted mice were kept on antibiotics for 2 weeks and analyzed after 5-8 weeks.

Tamoxifen-induced *in vivo* gene deletion

5 mg tamoxifen was applied by gavage on 5 consecutive days. Mice were analyzed after 4 weeks.

Hematopoietic stem cell transduction and adoptive transfer

BM cells were isolated from USP8$^{f/f}$CD4-Cre mice that were treated with 5-fluorouracil (150 mg/kg) for 72 h. After removal of red blood cells using lysis buffer, they were cultured in IMDM with 15% FCS in the presence of recombinant murine stem cell factor (50 ng/ml), recombinant murine IL-3 (20 ng/ml), and recombinant human IL-6 (50 ng/ml) (R&D Systems) for 48 h. On day 3 and 4 post isolation, 90' spin infections (1000g, 30ºC) were performed with retroviral supernatant in the presence of polybrene (5µg/ml) and cytokines. Cells were incubated for additional 4 h before medium was replaced. On day 5, 3x10^5 cells were injected into the eye vein of lethally irradiated (7Gy) Rag1-/- mice.

Microarray processing and data analysis.

RNA was isolated from sorted DP thymocytes using the RNeasy Mini kit (Quiagen) and RNA integrity was verified with a 2100 Bioanalyzer (Agilent Technologies). The samples were further processed for transcriptome analyses with the Agilent 4 × 44K whole mouse genome oligo expression microarray kit (Design ID 014868) according to the Agilent One-Color Microarray-Based Gene Expression Analysis protocol. The raw data were analyzed using GeneSpring GX 10.0 (normalization: shift to 75th percentile, baseline transformation: median of all samples). The normalized data were filtered to exclude probes flagged absent in all samples. The remaining probes were tested for statistical significance of expression using a two-sample Student's t-test (unpaired) with asymptotic p-value computation and a cut off of 0.05. Multiple testing correction was performed according to Benjamini Hochberg[53] ($P \leq 0.05$). The cutoff for the fold change is ≤ 2 (1 log2) up or down regulation.

Mass spectrometry (MS) analysis.

Protein IPs were generated from transfected HEK293T cells as described above, denatured in Laemmli buffer in the presence of 50 mM DTT and treated with 120 mM iodoacetamide (IAA, Sigma) for 10 minutes at RT maintaining neutral pH in the dark, followed by quenching with 40 mM DTT for 20 minutes in the dark. Subsequently, proteins were separated by SDS-PAGE and the protein band corresponding to the accumulated ubiquitin-modified 14-3-3β

molecule was excised. For in-gel digestion the excised gel band was destained with 30 % ACN, shrunk with 100 % ACN, and dried in a Vacuum Concentrator (Concentrator 5301, Eppendorf, Hamburg, Germany). Digests with trypsin and thermolysin were performed overnight at 37°C in 0.05 M NH_4HCO_3 (pH 8). About 0.1 µg of protease was used for one gel band. Peptides were extracted from the gel slices with 5 % formic acid. The digests were analyzed by nanoLC-MS/MS on a Q-TOF mass spectrometer (Agilent 6520, Agilent Technologies) and on a 6340 ion trap equipped with an ETD II source (Agilent Technologies). Both instruments were coupled to a 1200 Agilent nanoflow system via a HPLC-Chip cube ESI interface. Peptides were separated on a HPLC-Chip with an analytical column of 75 µm i.d. and 150 mm length and a 40-nL trap column, both packed with Zorbax 300SB C-18 (5 µm particle size). Peptides were eluted with a linear acetonitrile gradient with 1 %/min at a flow rate of 300 nL/min (starting with 3% acetonitrile).

The Q-TOF was operated in the 2 Ghz extended dynamic range mode. MS/MS analyses were performed using data-dependent acquisition mode. After a MS scan (2 spectra/s), a maximum of three peptides were selected for MS/MS (2 spectra/s). Singly charged precursor ions were excluded from selection. Internal calibration was applied using two reference masses.

ETD analyses on the ion trap were performed using data-dependent acquisition mode. After a MS scan (standard enhanced mode), a maximum of three peptides were selected for ETD-MS/MS (standard enhanced mode). The automated gain control (ICC) for MS scans was set to 350000. The maximum accumulation time was set to 300 ms. The following ETD parameters were used. ICC target: 400000, reaction time: 100 ms, cut-off: 140, resonance excitation (Smart Decomp) was used for doubly charged peptides.

Mascot Distiller 2.3 was used for raw data processing and for generating peak lists, essentially with standard settings for the Agilent Q-Tof and ion trap. Mascot Server 2.3 was used for database searching with the following parameters: peptide mass tolerance: 20 ppm for Q-Tof data and 1.1 Da for ion trap data, MS/MS mass tolerance: 0.05 Da for Q-Tof data and 0.3 Da for ion trap data, enzyme: “trypsin” with 3 uncleaved sites allowed for trypsin, and “none” for thermolysin, variable modifications: Carbamidomethyl (C), Gln->pyroGlu (N-term. Q), and oxidation (M) were used for all searches. In addition GG (K) and LRGG (K) were used as variable modifications for the identification of ubiquitination sites in the tryptic digest, and LRGG (K), LRLRGG (K) and VLRLRGG (K) were used for the thermolysin digest (thermolysin cleaves N-terminal of the amino acids L, I, F, A and V). For protein and peptide identification a custom database containing the protein sequences of 14-3-3β was used. All MS/MS spectra identified as ubiquitinated peptides were validated manually.

Statistical Analysis

We ensured that our sample sizes matched those generally employed in the field. Data were tested for normality applying the Kolmogorov-Smirnov test. If normality was given, a t-test was applied. Differences were considered significant for p values < 0.05.

Accession Code.

Microarray data were submitted to the GEO database (accession number: GSE55517).

Figure legends

Figure 1. USP8 interacts with GADS, 14-3-3β and the TCR signalosome. (a,b) HEK293T-cells were transfected with control or expression vectors for affinity-tagged USP8 and GADS **(a)** or 14-3-3β **(b)** as indicated. Anti-FLAG IP was performed. Lysates and precipitated proteins were analyzed by WB. The amount of precipitated GADS relative to the amount of precipitated USP8 was determined by densitometric analysis. Results shown are the means of 4 independent experiments ±SEM. **, $p<0.01$; ***, $p<0.001$ (unpaired, two-sided t-test). **(c)** Interaction of endogenous USP8 and GADS. Splenic $CD4^+$ WT T-cells were expanded for 4 days. Consequently, cells were starved, restimulated with anti-CD3/anti-CD28 Abs and lysed. Direct IP was performed with anti-USP8(X39) Ab. Lysates and precipitates were analyzed by WB. The amount of proteins present in the IP relative to the unstimulated control was determined by densitometric analysis. **(d)** HEK293T-cells were transfected with USP8-FLAG expression vectors. IP was performed and analyzed as in (a) using anti-FLAG and anti-14-3-3β Abs. **(e)** USP8 binds to TCR/CD28 signalosomes. $CD4^+$ T-cells were expanded as in (c). Signalosomes were purified after restimulation with Dynabeads® Mouse T-Activator CD3/CD28. Input and signalosome-associated proteins were analyzed by WB. **(f)** USP8 is processed upon TCR activation. $CD4^+$ T-cells were expanded and restimulated as in (c). Cell lysates were analyzed by WB. **(g)** Inhibition of USP8 processing in the presence of z-VAD. **(h)** USP8 modulates GADS and 14-3-3β ubiquitination. HEK293T-cells were transfected with the indicated vectors and lysates were analyzed as in (a). Experiments in Fig. 1 are representative of at least 3 independent trials.

Figure 2. Altered T-cell development in $USP8^{f/f}$CD4-Cre mice. (a) USP8 expression in $USP8^{f/f}$CD4-Cre thymocytes. Protein lysates were generated from $USP8^{f/f}$ and $USP8^{f/f}$CD4-Cre DP thymocytes. USP8 and Actin protein levels were determined by WB. **(b)** Left panels: Flow cytometric analysis of CD4 and CD8 expression on thymocytes derived from $USP8^{f/f}$, $USP8^{f/f}$CD4-Cre, and $USP8^{+/+}$CD4-Cre mice. Right panels: Total numbers of thymocyte subsets derived from 9-week-old $USP8^{f/f}$ and $USP8^{f/f}$CD4-Cre female mice. Results shown are the means of 3 independent experiments ±SEM and are representative of at least 3 independent trials. **(c)** Histology of thymi stained with hematoxilin and eosin (H&E). Scale bar: 400 µm. **(d)** Diminished thymic Treg and NKT levels. Left panel: percentages of $CD25^+Foxp3^+$ Tregs within the $CD4^+$ thymocyte population derived from $USP8^{f/f}$ and $USP8^{f/f}$CD4-Cre mice. Right panel: Representative flow cytometric analysis of $NK1.1^+/TCR\beta^+$ NKT-cells. Results shown are the means of 3 independent experiments ±SD. **(e)** Flow cytometric analysis of the surface markers TCRβ, CD69, CD62L, CD24 and CD5 on thymocyte subsets derived from $USP8^{f/f}$ and $USP8^{f/f}$CD4-Cre mice. Results shown are

representative of at least 6 independent experiments. DP, CD4/CD8 double positive; DN, CD4/CD8 double negative; SP4, CD4 single positive; SP8, CD8 single positive. *, $p<0.05$; **, $p<0.01$; ***, $p< 0.001$ (unpaired, two-sided t-test).

Figure 3. Diminished thymocyte proliferation upon USP8 depletion. (a) Impaired responsiveness of $USP8^{f/f}$CD4-Cre thymocytes to TCR- and PMA/IONO-induced proliferation. Thymocytes derived from $USP8^{f/f}$ and $USP8^{f/f}$CD4-Cre mice were stimulated for 72 h with plate-bound anti-CD3 Ab in the absence or presence of anti-CD28 Ab or IL-2, or with PMA/IONO. Expression of Ki67 and TCRβ were monitored by FACS analysis (left panels). Cell numbers were monitored in parallel (middle panel). Correlation of TCR and Ki67 expression is shown in the right panel for anti-CD3/CD28-stimulated thymocytes. Results are representative of at least 3 independent trials. **(b)** Impaired IL-2 production. Thymocytes derived from $USP8^{f/f}$ and $USP8^{f/f}$CD4-Cre mice were stimulated with plate-bound anti-CD3 Ab for 72h. IL-2 concentrations were determined in supernatants of stimulated cells and unstimulated controls. Results shown are the means of 3 independent experiments ±SD. *, $p< 0.05$ (unpaired, one-sided t-test). **(c)** Impairment of positive, but not negative thymic selection in $USP8^{f/f}$CD4-CreHY-TCR^{+} mice. Flow cytometric analysis of CD4 and CD8 expression on HY-TCR-positive thymocytes derived from 7-8-week-old female (upper panels) and male (lower panels) $USP8^{f/f}$HY-TCR^{+} and $USP8^{f/f}$CD4-CreHY-TCR^{+} mice. Results shown are one trial representative of at least 3 independent experiments.

Figure 4. Signaling defects in $USP8^{f/f}$CD4-Cre thymocytes. (a) Left panels: Flow cytometric analysis of IL-7Rα and CCR7 expression on thymocyte subsets derived from $USP8^{f/f}$ and $USP8^{f/f}$CD4-Cre mice. Results are representative of at least 3 independent experiments. Right panel: Relative IL-7Rα, CCR7 and CCND2 RNA expression in DP $USP8^{f/f}$CD4-Cre thymocytes. RNA expression was measured by quantitative real-time PCR analysis. Results shown are the mean mRNA levels in DP $USP8^{f/f}$CD4-Cre thymocytes relative to DP $USP8^{f/f}$ thymocytes ±SD for 4 independent experiments ($p<0.001$, unpaired, 2-sided t-test). **(b)** Foxo1 expression in $USP8^{f/f}$CD4-Cre thymocytes. Protein lysates were generated from anti-CD4-purified $USP8^{f/f}$ and $USP8^{f/f}$CD4-Cre thymocytes. Foxo1 and Actin protein levels were determined by WB. **(c)** CHIP analysis of Foxo1 binding to the *Il7r* locus in anti-CD4-purified $USP8^{f/f}$ and $USP8^{f/f}$CD4-Cre thymocytes. The data shown are representative of 3 independent experiments.

Figure 5. $USP8^{f/f}$CD4-Cre mice exhibit lymphopenia and hyperactivation of peripheral T-cells. (a) Left: Representative flow cytometric analysis of lymphocyte subsets in spleen derived from $USP8^{f/f}$, $USP8^{+/+}$CD4-Cre and $USP8^{f/f}$CD4-Cre mice. Percentages of CD3,

B220, CD4 and CD8 positive subsets are indicated. Percentages of CD44 and CD62L expression are shown for $CD3^+CD4^+$ lymphocytes. Right: Specific reduction of T-cell numbers in the spleen of $USP8^{f/f}$CD4-Cre mice. Total numbers of T- ($CD3^+$) and B-cells ($B220^+$) derived from $USP8^{f/f}$ and $USP8^{f/f}$CD4-Cre mice are shown. **(b)** Relative numbers of cells indicate Tregs ($CD25^+Foxp3^+$) referring to $CD4^+$cells; granulocytes ($Ly6G^+CD11b^+$) and monocytes ($CD115^+CD11b^+$) referring to $CD3^-$ cells, plasmacytoid dendritic cells ($CD11c^{lo}B220^+$) referring to $CD3^-Ly6C^+CD11b^-$ cells and conventional dendritic cells ($CD11c^{hi}Ly6C^-$) referring to $CD3^-MHCII^+$ cells. **(c)** Flow cytometric analysis of Tregs and pDCs in MLNs. Percentages are indicated as in (b). Results shown in a-c are the means of 6 independent experiments ±SD. **(d)** Cytokine profile of PMA/IONO-stimulated $CD4^+$ T-cells from spleen. IFNγ and IL-17 expression were monitored by intracellular staining and FACS analysis. **(e)** Flow cytometric analysis of the markers TCRβ, CD25, CD45RB and CD69 on $CD4^+$ (and $TCR\beta^+$ where indicated) lymphocytes derived from spleen and MLNs of $USP8^{f/f}$ or $USP8^{f/f}$CD4-Cre mice. Results shown in (d) and (e) are representative of at least 3 or 6 independent experiments, respectively. Tregs, regulatory T-cells; GCs, granulocytes; MCs, Monocytes; pDCs, plasmacytoid dendritic cells; cDCs, conventional dendritic cells. **, $p<0.01$; ***, $p< 0.001$ (unpaired, two-sided t-test).

Figure 6. T-cell specific USP8-deficiency causes lethal colitis. (a) Macroscopic images of bowel prolapses and intestines of $USP8^{f/f}$ and $USP8^{f/f}$CD4-Cre mice (upper left panels). Endoscopic recording (upper right panel), colons (lower left panel), and spleens and MLNs (lower right panel) of $USP8^{f/f}$ and diseased $USP8^{f/f}$CD4-Cre mice. **(b)** Survival curve of WT control mice and $USP8^{f/f}$CD4-Cre mice. **(c)** Left panels: Histology of colons from mice of the indicated genotypes stained with H&E, anti-CD3 Ab (pink) and anti-Foxp3 Ab (brown). Arrows indicate crypt abscess (top) and the presence of $Foxp3^+$ Tregs (bottom). Right panels: Colonic cryo-sections of mice of the indicated genotypes were immunostained with anti-CD11c, anti-myeloperoxidase (MPO) and anti-F4/80 Abs (red) to detect DCs, neutrophils and macrophages, respectively. Nuclei were counterstained with Hoechst 3342 (blue). Scale bar: 200 µm. **(d)** Histological analysis of splenic cell populations causing splenomegaly. H&E staining and labeling with anti-CD3, anti-B220, anti-Mac-3, and anti-Ki67 Abs was performed on splenic paraffin sections as indicated. Scale bar: 200 µm.

Figure 7. Intrinsic function of USP8 is critical for T-cell homeostasis. (a) Disturbed T-cell homeostasis upon peripheral USP8 deletion. Six week-old RAG2/Il2rg KO mice were intravenously injected with 12.5×10^6 splenocytes of the indicated genotypes. At day 4 post injection, mice were subjected to tamoxifen-induced gene deletion. On day 23 post injection, splenocytes were analyzed by FACS. Results are representative of 5 independent

experiments. **(b)** T-cell defect in mixed CD45.1$^+$WT/CD45.2$^+$USP8$^{f/f}$CD4-Cre BM chimeras. Reconstitution efficiency of the indicated T-cell subsets was monitored. Splenic CD4$^+$ T-cells were also stained for intracellular IFNγ and IL-17 upon PMA/IONO treatment. Data are representative of 3 independent experiments. **(c)** Time course of OHT-induced deletion of USP8. CD4$^+$ T-cells were enriched from spleens, stimulated with anti-CD3/anti-CD28 Abs in the presence of plate-bound anti-hamster Ab for 48 h and with IL-2 in the presence of OHT for the times indicated. Cells were analyzed for USP8 expression by WB and for CD3, CD4, CD8, and Ki67 expression by FACS. The results are representative of at least 3 independent experiments. **(d)** Essential role of USP8 catalytic activity and SH3 binding capacity. RAG1-/- mice were reconstituted with USP8$^{f/f}$CD4-Cre BMSCs transduced with retroviral particles expressing the indicated USP8 variants and eGFP. Mice were analyzed 8 weeks later for efficiency of CD4$^+$/eGFP$^+$ lymphocyte reconstitution. Results are representative of 3 independent experiments. Means ±SEM are shown in the middle panel. **, p<0.01; ***, p<0.001 (unpaired, 2-sided t-test). Right panel: Retroviral expression of ETAG-USP8 variants in NIH3T3 cells.

Figure 8. γδ T-cells promote colitis in the absence of functional Tregs. Dominance of γδ T-cells in colon epithelium **(a)** and MLNs **(b)** of USP8$^{f/f}$CD4-Cre mice. IELs and MLN cells were prepared from USP8$^{f/f}$ and diseased USP8$^{f/f}$CD4-Cre mice and analyzed by FACS. The data shown are representative of 2 independent experiments. **(c)** Total numbers of αβ and γδ T-cells in MLNs of 12-week-old USP8$^{f/f}$ or USP8$^{f/f}$CD4-Cre mice, or CD45.1$^+$WT/ CD45.2$^+$USP8$^{f/f}$CD4-Cre BM chimera (normalized to 100% reconstitution efficiency for each genotype). ***, p<0.001 (unpaired, two-sided t-test). **(d)** Cytokine levels in serum from aged USP8$^{f/f}$ and USP8$^{f/f}$CD4-Cre mice with overt signs of colitis. *, p<0.05 (unpaired, two-sided t-test). **(e)** Lack of *in vivo* Treg function. Rag1-/- mice were injected with USP8$^{f/f}$ naïve T-cells in the absence or presence of USP8$^{f/f}$ (WT) or USP8$^{f/f}$CD4-Cre (KO) Tregs. After 9 weeks, splenic CD4$^+$ cell were analyzed for Foxp3 expression. Colons were analyzed macroscopically and by H&E staining of distal paraffin sections. Results are representative of at least 3 independent experiments. **(f)** Lack of *in vitro* Treg function. Division of anti-CD3-stimulated Tresp cells cultured in the presence or absence of USP8$^{f/f}$ or USP8$^{f/f}$CD4-Cre Treg cells was assessed by dilution of CFSE. Data are representative of 2 independent experiments, each performed in triplicates with cells derived from 4 USP8$^{f/f}$ mice and 10 USP8$^{f/f}$CD4-Cre mice. **(g)** Deregulated IFNγ response in splenic USP8$^{f/f}$CD4-Cre Tregs. IFNγ expression in PMA/IONO-stimulated CD4$^+$Foxp3$^+$ splenocytes from 7-week-old USP8$^{f/f}$ and USP8$^{f/f}$CD4-Cre mice. Results are representative of 5 independent experiments. **, p<0.01 (paired, 2-sided t-test).

Supplementary Figure Legends

Supplementary Figure S1. Identification of USP8-interacting proteins by Y2H screening. (a) Schematic representation of USP8 baits: Bait 1 (residues 143 – 485 of human USP8) encodes the N-terminal SH3BM. Bait 2 (residues 481-764) harbors the 14-3-3BM and the C-terminal SH3BM. **(b)** NMY51 cells were cotransformed with vectors encoding bait 1 or 2 and either GADS or 14-3-3β. The interaction between the proteins was confirmed by yeast growth on agar plates lacking tryptophane, leucine and histidine (-TLH) and by β-Galactosidase assay (X-Gal). As a control, LaminC was coexpressed with GADS and 14-3-3β, respectively.

Supplementary Figure S2. USP8 modulates GADS and 14-3-3β ubiquitination. (a) HEK293T-cells were transfected with an empty vector or expression vectors for FLAG-tagged USP8 and/or FLAG-tagged ubiquitin, HA-tagged GADS or HA-tagged 14-3-3β as indicated on the top. IP was performed with anti-HA(3F10) Ab. Lysates were immunoblotted with anti-FLAG and anti-HA(3F10) Abs, precipitated proteins with anti-HA(3F10) Ab. *, ubiquitin modification. Results are representative of 2 independent experiments. **(b)** MS analysis of 14-3-3β ubiquitination sites. Flag-tagged USP8(C786A) was cotransfected with FLAG-ubiquitin and HA-tagged 14-3-3β in 293HEK cells. An anti-HA-IP was performed and the isolated proteins were separated by SDS-PAGE. A protein band corresponding to the accumulated ubiquitin-modified 14-3-3β molecule was excised and analyzed as described in *Materials and Methods*. Briefly, proteins were digested in gel in separate experiments with trypsin and with thermolysin. Both digests were analyzed with CID on a Q-TOF instrument and with ETD on an ion trap instrument. The peptide MDKSELVQKAK generated in the thermolysin digest was identified on both instruments with an N-terminal acetylation, an oxidized methionine and with a lysine linked to LRGG. The shown ETD spectrum allows unambiguous localization of the ubiquitination site to K-9. The peptide VFYYEILNSPEKACS (also generated in the thermolysin digest) was identified by CID on the Q-Tof instrument with a carbamidomethylated cysteine and a LRGG-modified lysine residue. The shown CID spectrum allowed unambiguous localization of the ubiquitination site to position 189.

Supplementary Figure S3. Consequences of USP8 gene deletion in thymocytes. (a) Verification of USP8 gene deletion in thymocytes of $USP8^{f/f}$CD4-Cre mice by Southern blot analysis. Genomic DNA from sorted thymocytes derived from WT and $USP8^{f/f}$CD4-Cre mice was digested with NcoI and analyzed using a ^{32}P-labeled probe. Efficient deletion is indicated by appearance of the 6 kb KO band at the expense of the 5 kb band representing the floxed allele. **(b)** USP8 protein expression in thymocyte subsets of $USP8^{f/f}$ (c) and $USP8^{f/f}$CD4-Cre (KO) mice. DN, SP4 and SP8 thymocyte subsets were sorted for WB analysis. **(c)** USP8

protein expression in thymocyte subsets of USP8$^{f/f}$ (c) and USP8$^{f/f}$LCK^{Cre} (KO) mice. DN, DP, SP4 and SP8 thymocyte subsets were sorted for WB analysis. **(d)** CD25 and CD44 expression on DN thymocytes for analysis of the early DN1 (CD44^{+}CD25^{-}), DN2 (CD44^{+}CD25^{+}), DN3 CD(CD44^{-}CD25^{+}) and DN4(CD44^{-}CD25^{-}) stages of thymocyte development. **(e)** Developmental defect in USP8$^{f/f}$LCK^{Cre} thymocytes. Upper panels: Flow cytometric analysis of CD4 and CD8 expression on thymocytes derived from USP8$^{f/f}$ and USP8$^{f/f}$LCK^{Cre} mice. Lower panels: TCRβ expression on thymocyte subsets of USP8$^{f/f}$ and USP8$^{f/f}$LCK^{Cre} mice. Results in (d) and (e) are representative of 3 independent experiments. **(f)** Thymocyte survival assay. Thymocytes derived from USP8$^{f/f}$ and USP8$^{f/f}$CD4-Cre mice were stimulated as in figure 3a for 48 h and stained with propidium iodide (PI) and a fluorescent conjugate of Annexin V. The percentages of cells in early apoptosis (AnnexinV^{+}PI^{-}) and late apoptosis (AnnexinV^{+}PI^{+}) are indicated. Results in (f) are the means of 3 independent experiments ±SD.

Supplementary Figure S4. Normal TCR signaling in USP8$^{f/f}$CD4-Cre thymocytes. (a,b) Normal levels of STAM2 expression and ubiquitination in CD4^{+} thymocytes. **(a)** Protein lysates from thymocytes were analyzed by WB for USP8 and STAM2 expression. **(b)** Protein lysates from anti-CD4-purified thymocytes were analyzed by WB for expression levels of proteins harboring K48-linked and K63-linked ubiquitin chains. **(c)** Ligand-induced TCR downmodulation. Thymocytes were stained on ice with biotinylated hamster anti-TCRβ Ab. Subsequently, the TCR was crosslinked with anti-hamster Ab at 37ºC for the indicated times. Remaining surface TCR was labeled with streptavidin-PE and measured by FACS in SP4 (left) and DP gates. The percentages of surface expression are presented as the mean fluorescence values of treated cells, using the untreated controls as reference (n=5). **(d-i)** Total thymocytes **(d,e,i)** or enriched DP thymocytes **(f,g,h)** were stimulated for the indicated times with anti-CD3/anti-CD28 Abs. Phosphorylation of ERK1/2, JNK, p38, Akt **(d)** and IκBα **(e)**, and Actin protein levels were monitored by WB. In **(f)**, IκBα, 14-3-3β, GADS and Actin protein levels were monitored by WB. **(g,h)** NF-κB activation and AP1 activation were determined by EMSA. **(i)** Tyrosine phosphorylation was detected by WB with the PY20 anti-phosphotyrosine Ab. Total protein levels correspond to the Actin levels shown in (d). **(j)** Ca^{2+} influx in anti-CD3/anti-CD28-stimulated, enriched DP thymocytes. Thymocytes were loaded with indo-1-AM (5 μg/ml) and activated with anti-CD3/anti-CD28. The graph shows the ratio of bound to unbound indo-1-AM as a measure of Ca^{2+} influx. Results are representative of at least 3 independent experiments. SFo, surface fluorescence.

Supplementary Figure S5. Microarray analysis of gene expression in DP thymocytes upon USP8 depletion. (a) Microarray analysis of 2 groups of 2 USP8$^{f/f}$ and 2 USP8$^{f/f}$CD4-Cre DP thymocyte populations (8 mice in total), which resulted in a list of 74 genes with a

significant >2-fold difference. The heatmap of the 74 gene list is shown. **(b)** Top Network extracted by analysis of the microarray gene expression data using the Ingenuity software.

Supplementary Figure S6. Consequences of USP8 gene deletion in peripheral T-cells. **(a)** Representative flow cytometric analysis of lymphocyte subsets in MLNs derived from $USP8^{f/f}$, $USP8^{+/+}$CD4-Cre and $USP8^{f/f}$CD4-Cre mice was performed as in Fig. 5a (n>6). **(b)** USP8 gene deletion in peripheral T-cells from $USP8^{f/f}$CD4-Cre mice. Southern blot analysis was performed using sorted $CD4^+$ and $CD8^+$ cells from spleen and MLNs derived from WT and $USP8^{f/f}$CD4-Cre mice. **(c)** Normal USP8 and Foxo1 protein expression in sorted effector T-cells derived from $USP8^{f/f}$ and $USP8^{f/f}$CD4-Cre mice. **(d)** IL7Rα expression on $USP8^{f/f}$CD4-Cre effector and naïve T-cells. $CD3^+CD4^+$ splenocytes were analyzed for CD44, CD62L and IL7Rα expression to determine IL7Rα expression on effector and naïve T-cell subsets. (n=5; p=0.006; paired, 2-sided, t-test). **(e)** Altered T-cell homeostasis in $USP8^{f/f}LCK^{Cre}$ mice. Percentages of $CD3^+$, $CD4^+$, and $CD8^+$ lymphocytes and the distribution of naïve ($CD44^{lo}CD62L^{hi}$) and effector T-cells ($CD44^{hi}CD62L^{lo}$) within the $CD3^+/CD4^+$ population were determined in spleen (n=3). The percentages of IL7Rα expressing naïve T-cells are indicated in the right panel. Results shown are the means of 4 independent experiments ±SD. **, p<0.01 (unpaired, 2-sided t-test). **(f)** Representative FACS analysis of CCR7 expression on $CD4^+$ splenocytes derived from $USP8^{f/f}$ and $USP8^{f/f}$CD4-Cre mice (n=3). **(g)** Upper panels: Representative IL-7Rα expression on SP4 and SP8 thymocytes derived from BM chimera reconstituted with $CD45.1^+$ WT and $CD45.2^+$ $USP8^{f/f}$CD4-Cre cells (n=6). Lower panel: percentages of IL7Rα expressing naïve T-cells in $CD45.1^+$WT/$CD45.2^+USP8^{f/f}$CD4-Cre BM chimera. Results shown are the means of 6 independent experiments ±SD.

Supplementary Figure S7. Proximal TCR signaling is not affected by OHT-induced USP8 deletion. (a-d) $CD4^+$ T-cells were enriched from spleens of $USP8^{+/f}$CD4-$CreER^{T2}$ (control) and $USP8^{f/f}$CD4-$CreER^{T2}$ (iKO) mice, expanded and treated with OHT for 48 h as in Figure 7c. Subsequently, cells were starved for 2 h and restimulated with anti-CD3 and anti-CD28 Abs for the times indicated. **(a)** Assessment of USP8, LAT phospho-LAT, phospho-PLCγ, phospho-ERK1/2 and Actin expression levels by WB. **(b)** Cells were also pretreated with MG132 and chloroquine to inhibit proteasomal and lysosomal degradation, respectively. USP8, GADS, 14-3-3β, phospho-IκBα, and Actin expression were monitored by WB. **(c)** Cell lysates were analyzed for Actin and USP8 expression. In parallel, p38- and PKB-phosphorylation was monitored using phospho-specific Abs. **(d)** Analysis of the levels of USP8, proteins modified by K48-linked ubiquitination, tyrosine-phosphorylated proteins, SLP76, SLP76 phosphorylated at S376 (14-3-3BM), phospho-JNK, Foxo1, GRAIL and Actin by WB. The results shown in Supplementary Fig. 7 are representative of at least 3 independent experiments.

Supplementary Figure S8. TCR signalosome formation upon OHT-induced USP8 deletion and USP8 binding to the CD3/CD28 cluster in Jurkat-derived KO cells. (a) $CD4^+$ T-cells were enriched from spleens of $USP8^{+/f}$CD4-$CreER^{T2}$ (control) and $USP8^{f/f}$CD4-$CreER^{T2}$ (iKO) mice, expanded and treated with OHT for 48 h as in Figure 7c. Subsequently, TCR signalosomes were purified after restimulation with Dynabeads® Mouse T-Activator CD3/CD28. Total lysate (input) and components of the signaling complex were analyzed by WB using Abs directed against USP8, tyrosine-phosphorylated proteins, CD3ε and the indicated signaling components. **(b)** Jurkat-derived GADS- (dG32GADS-/-), LAT- (J.Cam2.5), and SLP76 (J14) KO cells were stimulated with Dynabeads® Human T-Activator CD3/CD28 prior to purification of TCR signalosomes. Antibodies directed against USP8 and TCR-proximal signaling components were used to analyze the input and purified signalosome components. Results are representative of 3 independent experiments.

Supplementary Movie S1 (3.8Mb). Typical appearance of healthy colon visualized by *in vivo* mini-endoscopic analysis of $USP8^{f/f}$ mouse.

Supplementary Movie S2 (4.1Mb). Endoscopic recording of $USP8^{f/f}$CD4-Cre colon revealing typical signs of colitis like enhanced granularity, loss of the vascular pattern of the mucosa and a reduction in translucency.

1. Sun SC. Deubiquitylation and regulation of the immune response. *Nature reviews Immunology* 2008, **8**(7)**:** 501-511.

2. Jiang X, Chen ZJ. The role of ubiquitylation in immune defence and pathogen evasion. *Nature reviews Immunology* 2012, **12**(1)**:** 35-48.

3. Komander D, Clague MJ, Urbe S. Breaking the chains: structure and function of the deubiquitinases. *Nature reviews Molecular cell biology* 2009, **10**(8)**:** 550-563.

4. Harhaj EW, Dixit VM. Regulation of NF-kappaB by deubiquitinases. *Immunological reviews* 2012, **246**(1)**:** 107-124.

5. Niendorf S, Oksche A, Kisser A, Lohler J, Prinz M, Schorle H*, et al.* Essential role of ubiquitin-specific protease 8 for receptor tyrosine kinase stability and endocytic trafficking in vivo. *Molecular and cellular biology* 2007, **27**(13)**:** 5029-5039.

6. Wright MH, Berlin I, Nash PD. Regulation of endocytic sorting by ESCRT-DUB-mediated deubiquitination. *Cell biochemistry and biophysics* 2011, **60**(1-2)**:** 39-46.

7. Kato M, Miyazawa K, Kitamura N. A deubiquitinating enzyme UBPY interacts with the Src homology 3 domain of Hrs-binding protein via a novel binding motif PX(V/I)(D/N)RXXKP. *The Journal of biological chemistry* 2000, **275**(48)**:** 37481-37487.

8. Reincke M, Sbiera S, Hayakawa A, Theodoropoulou M, Osswald A, Beuschlein F*, et al.* Mutations in the deubiquitinase gene USP8 cause Cushing's disease. *Nature genetics* 2014.

9. Mizuno E, Kitamura N, Komada M. 14-3-3-dependent inhibition of the deubiquitinating activity of UBPY and its cancellation in the M phase. *Experimental cell research* 2007, **313**(16)**:** 3624-3634.

10. Berry DM, Nash P, Liu SK, Pawson T, McGlade CJ. A high-affinity Arg-X-X-Lys SH3 binding motif confers specificity for the interaction between Gads and SLP-76 in T cell signaling. *Current biology : CB* 2002, **12**(15)**:** 1336-1341.

11. Harkiolaki M, Lewitzky M, Gilbert RJ, Jones EY, Bourette RP, Mouchiroud G*, et al.* Structural basis for SH3 domain-mediated high-affinity binding between Mona/Gads and SLP-76. *The EMBO journal* 2003, **22**(11)**:** 2571-2582.

12. Kaneko T, Kumasaka T, Ganbe T, Sato T, Miyazawa K, Kitamura N*, et al.* Structural insight into modest binding of a non-PXXP ligand to the signal transducing adaptor molecule-2 Src homology 3 domain. *The Journal of biological chemistry* 2003, **278**(48)**:** 48162-48168.

13. Brownlie RJ, Zamoyska R. T cell receptor signalling networks: branched, diversified and bounded. *Nature reviews Immunology* 2013, **13**(4)**:** 257-269.

14. Heissmeyer V, Vogel KU. Molecular control of Tfh-cell differentiation by Roquin family proteins. *Immunological reviews* 2013, **253**(1)**:** 273-289.

15. Naik E, Webster JD, DeVoss J, Liu J, Suriben R, Dixit VM. Regulation of proximal T cell receptor signaling and tolerance induction by deubiquitinase Usp9X. *The Journal of experimental medicine* 2014, **211**(10)**:** 1947-1955.

16. Zou Q, Jin J, Hu H, Li HS, Romano S, Xiao Y*, et al.* USP15 stabilizes MDM2 to mediate cancer-cell survival and inhibit antitumor T cell responses. *Nature immunology* 2014, **15**(6)**:** 562-570.

17. Soares L, Seroogy C, Skrenta H, Anandasabapathy N, Lovelace P, Chung CD*, et al.* Two isoforms of otubain 1 regulate T cell anergy via GRAIL. *Nature immunology* 2004, **5**(1)**:** 45-54.

18. Mackall CL, Fry TJ, Gress RE. Harnessing the biology of IL-7 for therapeutic application. *Nature reviews Immunology* 2011, **11**(5)**:** 330-342.

19. Kerdiles YM, Beisner DR, Tinoco R, Dejean AS, Castrillon DH, DePinho RA*, et al.* Foxo1 links homing and survival of naive T cells by regulating L-selectin, CCR7 and interleukin 7 receptor. *Nature immunology* 2009, **10**(2)**:** 176-184.

20. Ouyang W, Beckett O, Flavell RA, Li MO. An essential role of the Forkhead-box transcription factor Foxo1 in control of T cell homeostasis and tolerance. *Immunity* 2009, **30**(3)**:** 358-371.

21. Takada K, Jameson SC. Naive T cell homeostasis: from awareness of space to a sense of place. *Nature reviews Immunology* 2009, **9**(12)**:** 823-832.

22. Ouyang W, Liao W, Luo CT, Yin N, Huse M, Kim MV*, et al.* Novel Foxo1-dependent transcriptional programs control T(reg) cell function. *Nature* 2012, **491**(7425)**:** 554-559.

23. Obsil T, Obsilova V. Structural basis of 14-3-3 protein functions. *Seminars in cell & developmental biology* 2011, **22**(7)**:** 663-672.

24. Tzivion G, Dobson M, Ramakrishnan G. FoxO transcription factors; Regulation by AKT and 14-3-3 proteins. *Biochimica et biophysica acta* 2011, **1813**(11)**:** 1938-1945.

25. Surh CD, Sprent J. Homeostasis of naive and memory T cells. *Immunity* 2008, **29**(6)**:** 848-862.

26. Park SG, Mathur R, Long M, Hosh N, Hao L, Hayden MS*, et al.* T regulatory cells maintain intestinal homeostasis by suppressing gammadelta T cells. *Immunity* 2010, **33**(5)**:** 791-803.

27. Schamel WW, Alarcon B. Organization of the resting TCR in nanoscale oligomers. *Immunological reviews* 2013, **251**(1)**:** 13-20.

28. Lasserre R, Cuche C, Blecher-Gonen R, Libman E, Biquand E, Danckaert A*, et al.* Release of serine/threonine-phosphorylated adaptors from signaling microclusters down-regulates T cell activation. *The Journal of cell biology* 2011, **195**(5)**:** 839-853.

29. Anderson G, Hare KJ, Jenkinson EJ. Positive selection of thymocytes: the long and winding road. *Immunology today* 1999, **20**(10)**:** 463-468.

30. Orban PC, Chui D, Marth JD. Tissue- and site-specific DNA recombination in transgenic mice. *Proceedings of the National Academy of Sciences of the United States of America* 1992, **89**(15)**:** 6861-6865.

31. Yoder J, Pham C, Iizuka YM, Kanagawa O, Liu SK, McGlade J*, et al.* Requirement for the SLP-76 adaptor GADS in T cell development. *Science* 2001, **291**(5510)**:** 1987-1991.

32. Sledzinska A, Hemmers S, Mair F, Gorka O, Ruland J, Fairbairn L*, et al.* TGF-beta Signalling Is Required for CD4(+) T Cell Homeostasis But Dispensable for Regulatory T Cell Function. *PLoS biology* 2013, **11**(10)**:** e1001674.

33. Vantourout P, Hayday A. Six-of-the-best: unique contributions of gammadelta T cells to immunology. *Nature reviews Immunology* 2013, **13**(2)**:** 88-100.

34. Ketscher L, Hannss R, Morales DJ, Basters A, Guerra S, Goldmann T*, et al.* Selective inactivation of USP18 isopeptidase activity in vivo enhances ISG15 conjugation and viral resistance. *Proceedings of the National Academy of Sciences of the United States of America* 2015.

35. De A, Dainichi T, Rathinam CV, Ghosh S. The deubiquitinase activity of A20 is dispensable for NF-kappaB signaling. *EMBO reports* 2014, **15**(7)**:** 775-783.

36. Lu TT, Onizawa M, Hammer GE, Turer EE, Yin Q, Damko E*, et al.* Dimerization and ubiquitin mediated recruitment of A20, a complex deubiquitinating enzyme. *Immunity* 2013, **38**(5)**:** 896-905.

37. Wang X, Li JP, Chiu LL, Lan JL, Chen DY, Boomer J*, et al.* Attenuation of T cell receptor signaling by serine phosphorylation-mediated lysine 30 ubiquitination of SLP-76 protein. *The Journal of biological chemistry* 2012, **287**(41)**:** 34091-34100.

38. Nurieva RI, Zheng S, Jin W, Chung Y, Zhang Y, Martinez GJ*, et al.* The E3 ubiquitin ligase GRAIL regulates T cell tolerance and regulatory T cell function by mediating T cell receptor-CD3 degradation. *Immunity* 2010, **32**(5)**:** 670-680.

39. McCaughtry TM, Etzensperger R, Alag A, Tai X, Kurtulus S, Park JH*, et al.* Conditional deletion of cytokine receptor chains reveals that IL-7 and IL-15 specify CD8 cytotoxic lineage fate in the thymus. *The Journal of experimental medicine* 2012, **209**(12)**:** 2263-2276.

40. Ouyang W, Beckett O, Ma Q, Paik JH, DePinho RA, Li MO. Foxo proteins cooperatively control the differentiation of Foxp3+ regulatory T cells. *Nature immunology* 2010, **11**(7)**:** 618-627.

41. Nanno M, Kanari Y, Naito T, Inoue N, Hisamatsu T, Chinen H*, et al.* Exacerbating role of gammadelta T cells in chronic colitis of T-cell receptor alpha mutant mice. *Gastroenterology* 2008, **134**(2)**:** 481-490.

42. Gubbels Bupp MR, Edwards B, Guo C, Wei D, Chen G, Wong B*, et al.* T cells require Foxo1 to populate the peripheral lymphoid organs. *European journal of immunology* 2009, **39**(11)**:** 2991-2999.

43. Rubtsov YP, Rasmussen JP, Chi EY, Fontenot J, Castelli L, Ye X*, et al.* Regulatory T cell-derived interleukin-10 limits inflammation at environmental interfaces. *Immunity* 2008, **28**(4)**:** 546-558.

44. Fontenot JD, Rasmussen JP, Gavin MA, Rudensky AY. A function for interleukin 2 in Foxp3-expressing regulatory T cells. *Nature immunology* 2005, **6**(11)**:** 1142-1151.

45. Forster R, Davalos-Misslitz AC, Rot A. CCR7 and its ligands: balancing immunity and tolerance. *Nature reviews Immunology* 2008, **8**(5)**:** 362-371.

46. Garcia S, DiSanto J, Stockinger B. Following the development of a CD4 T cell response in vivo: from activation to memory formation. *Immunity* 1999, **11**(2)**:** 163-171.

47. Lee PP, Fitzpatrick DR, Beard C, Jessup HK, Lehar S, Makar KW*, et al.* A critical role for Dnmt1 and DNA methylation in T cell development, function, and survival. *Immunity* 2001, **15**(5)**:** 763-774.

48. Kisielow P, Bluthmann H, Staerz UD, Steinmetz M, von Boehmer H. Tolerance in T-cell-receptor transgenic mice involves deletion of nonmature CD4+8+ thymocytes. *Nature* 1988, **333**(6175)**:** 742-746.

49. Lugassy J, Corso J, Beach D, Petrik T, Oellerich T, Urlaub H*, et al.* Modulation of TCR responsiveness by the Grb2-family adaptor, Gads. *Cellular signalling* 2015, **27**(1)**:** 125-134.

50. Larghi P, Williamson DJ, Carpier JM, Dogniaux S, Chemin K, Bohineust A*, et al.* VAMP7 controls T cell activation by regulating the recruitment and phosphorylation of vesicular Lat at TCR-activation sites. *Nature immunology* 2013, **14**(7)**:** 723-731.

51. Yeh WC, Shahinian A, Speiser D, Kraunus J, Billia F, Wakeham A*, et al.* Early lethality, functional NF-kappaB activation, and increased sensitivity to TNF-induced cell death in TRAF2-deficient mice. *Immunity* 1997, **7**(5)**:** 715-725.

52. Lahl K, Loddenkemper C, Drouin C, Freyer J, Arnason J, Eberl G*, et al.* Selective depletion of Foxp3+ regulatory T cells induces a scurfy-like disease. *The Journal of experimental medicine* 2007, **204**(1)**:** 57-63.

53. Klipper-Aurbach Y, Wasserman M, Braunspiegel-Weintrob N, Borstein D, Peleg S, Assa S*, et al.* Mathematical formulae for the prediction of the residual beta cell function during the first two years of disease in children and adolescents with insulin-dependent diabetes mellitus. *Medical hypotheses* 1995, **45**(5)**:** 486-490.

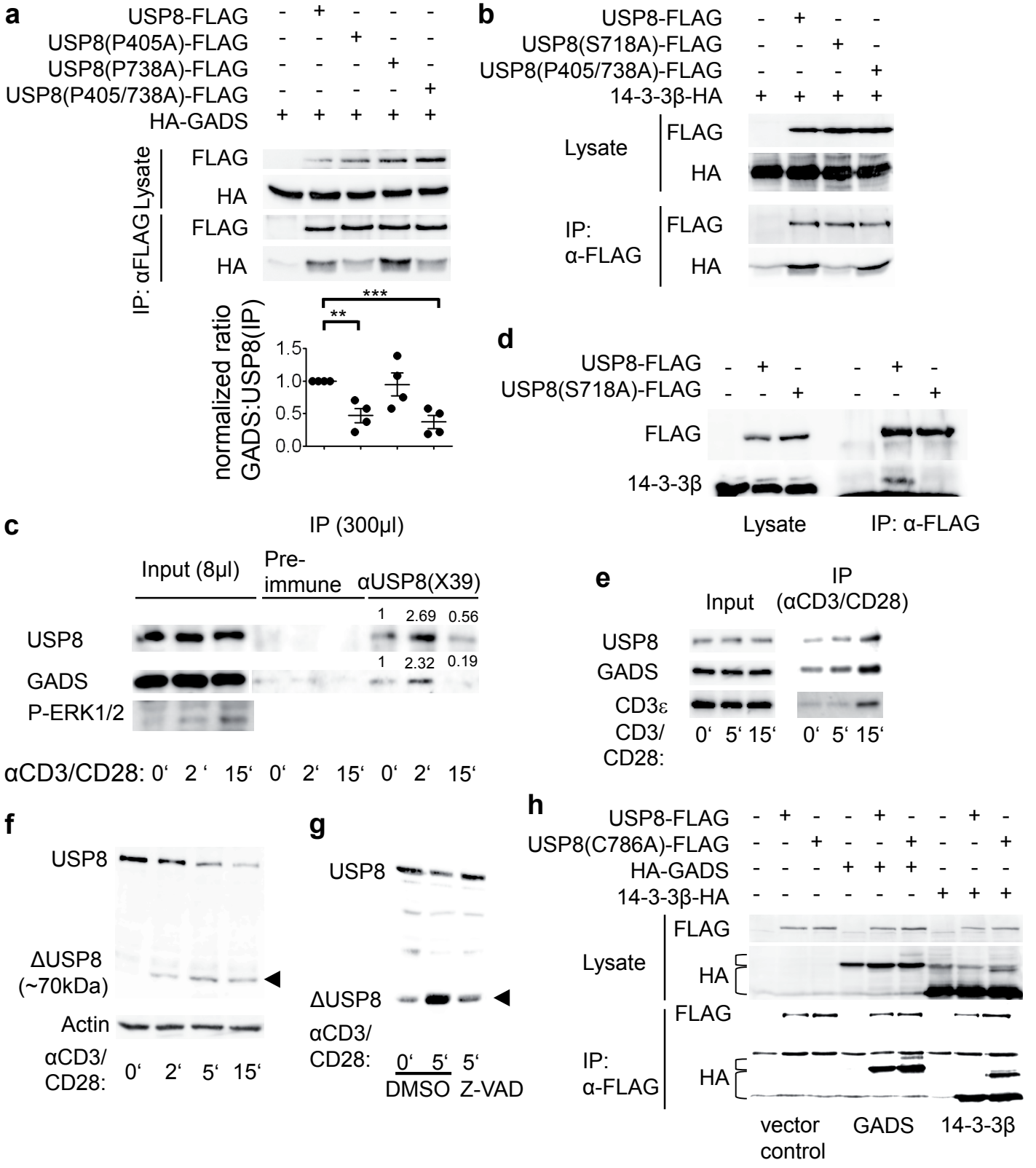

Dufner et al., Fig. 1

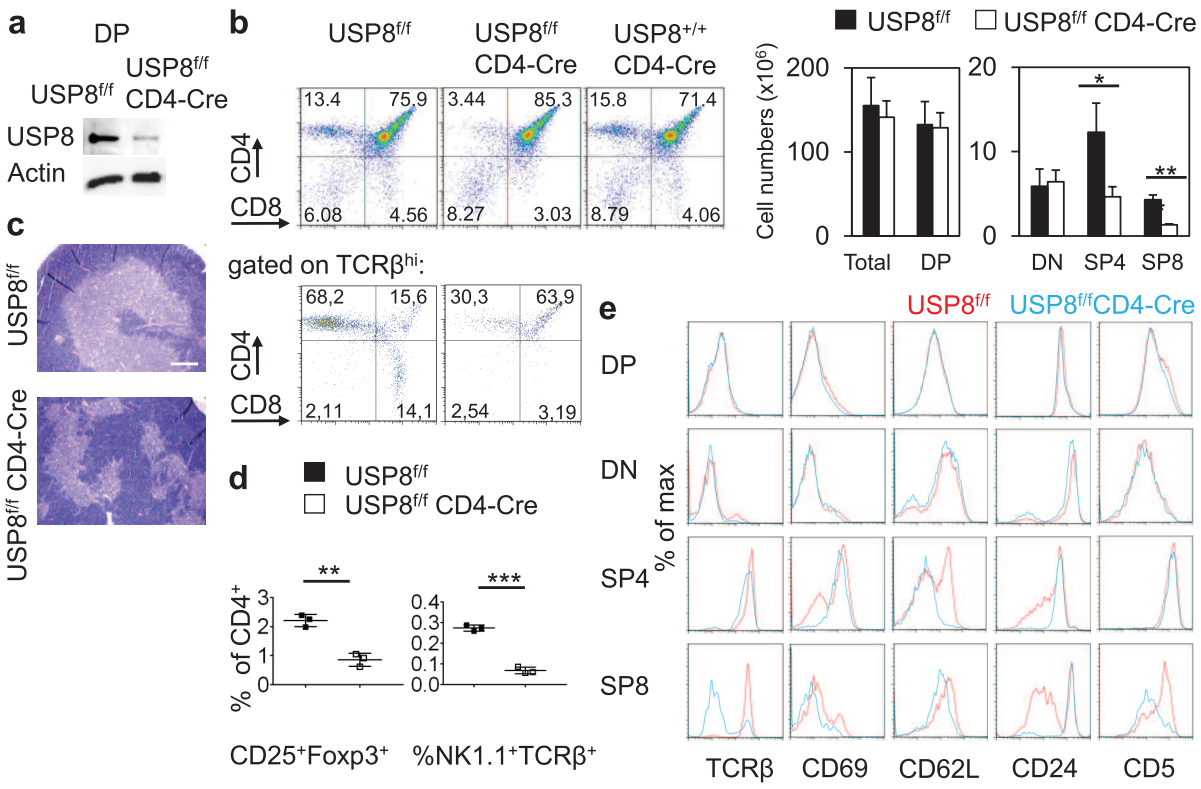

Dufner et al., Fig. 2

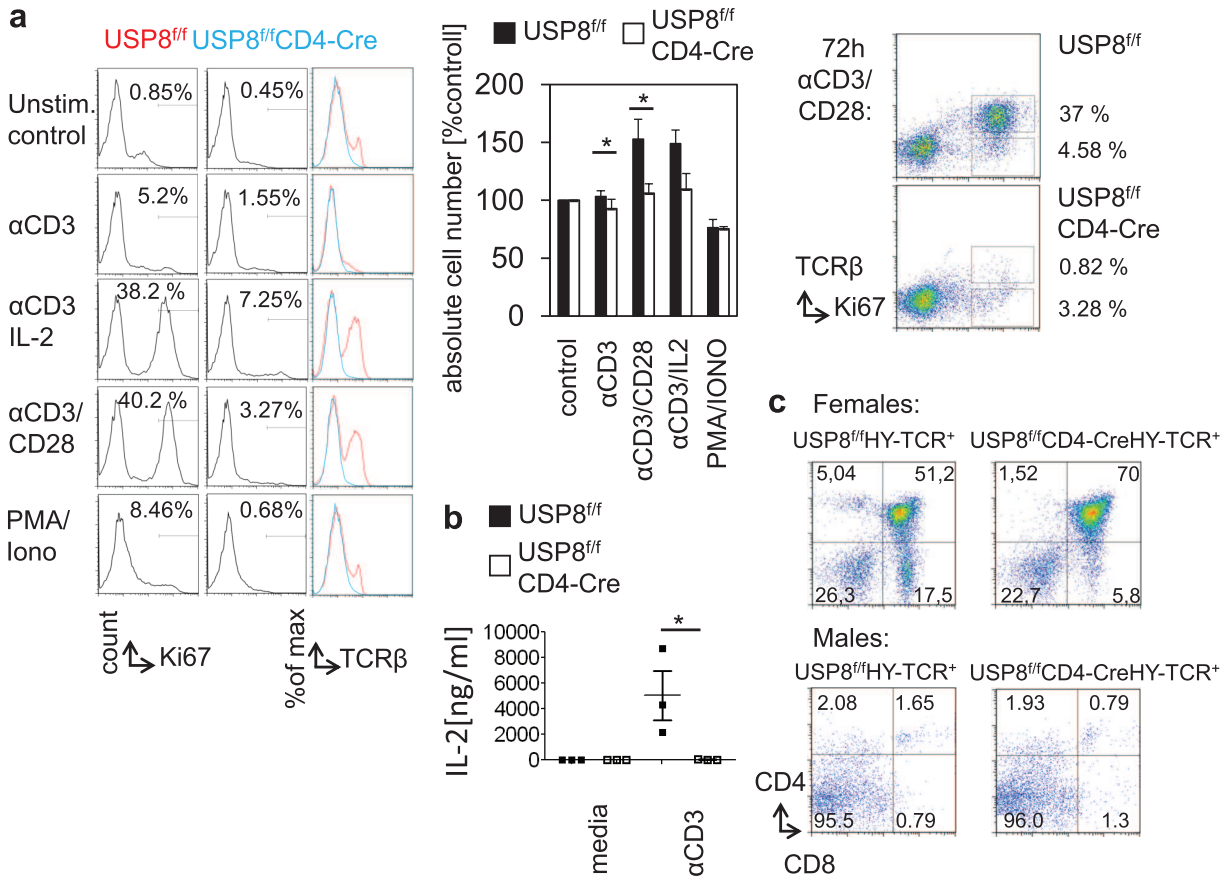

Dufner et al., Fig. 3

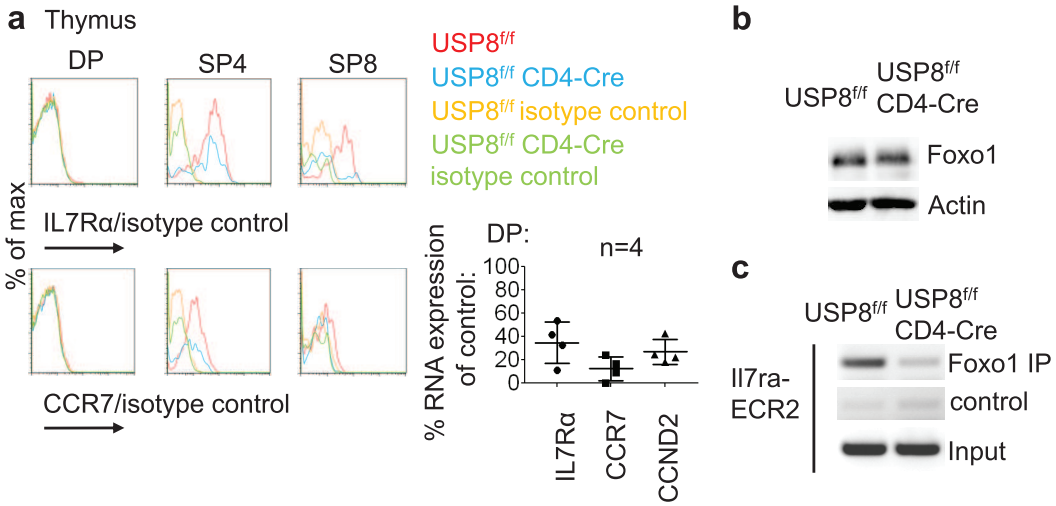

Dufner et al., Fig. 4

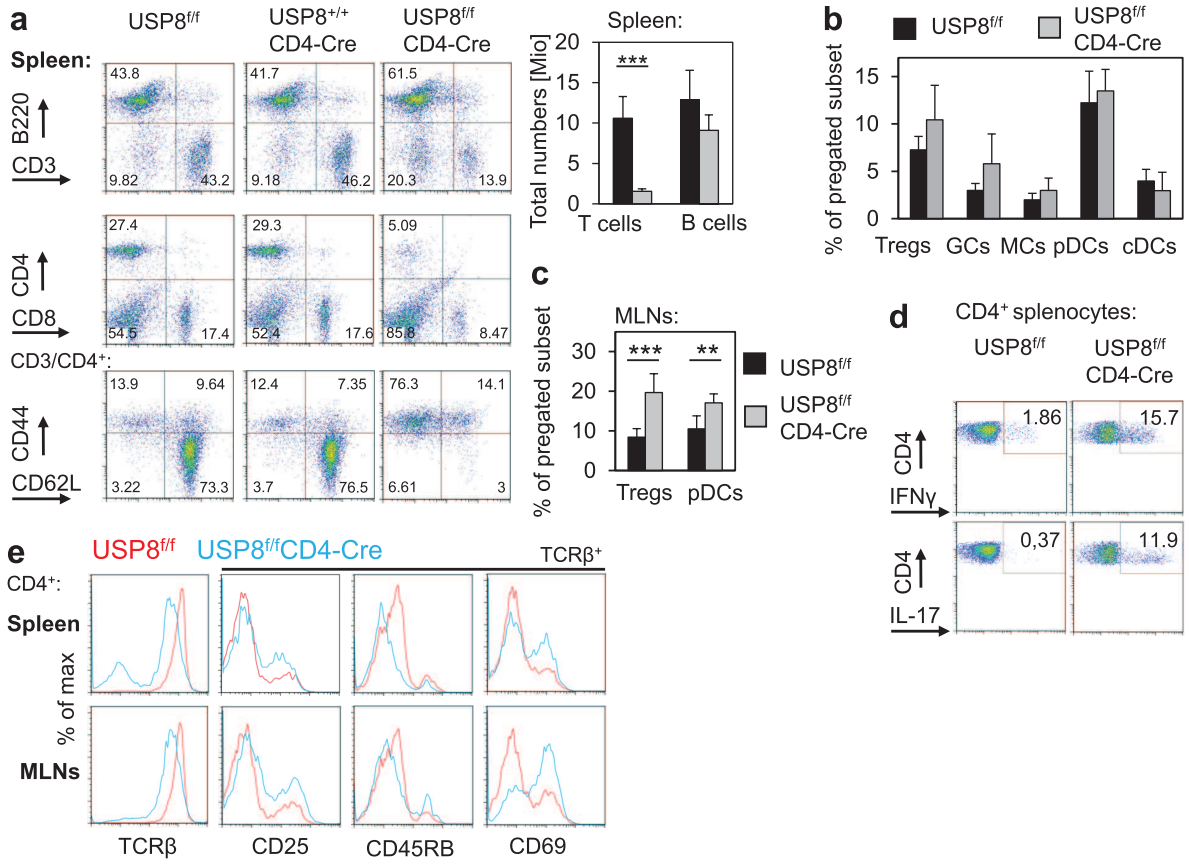

Dufner et al., Fig. 5

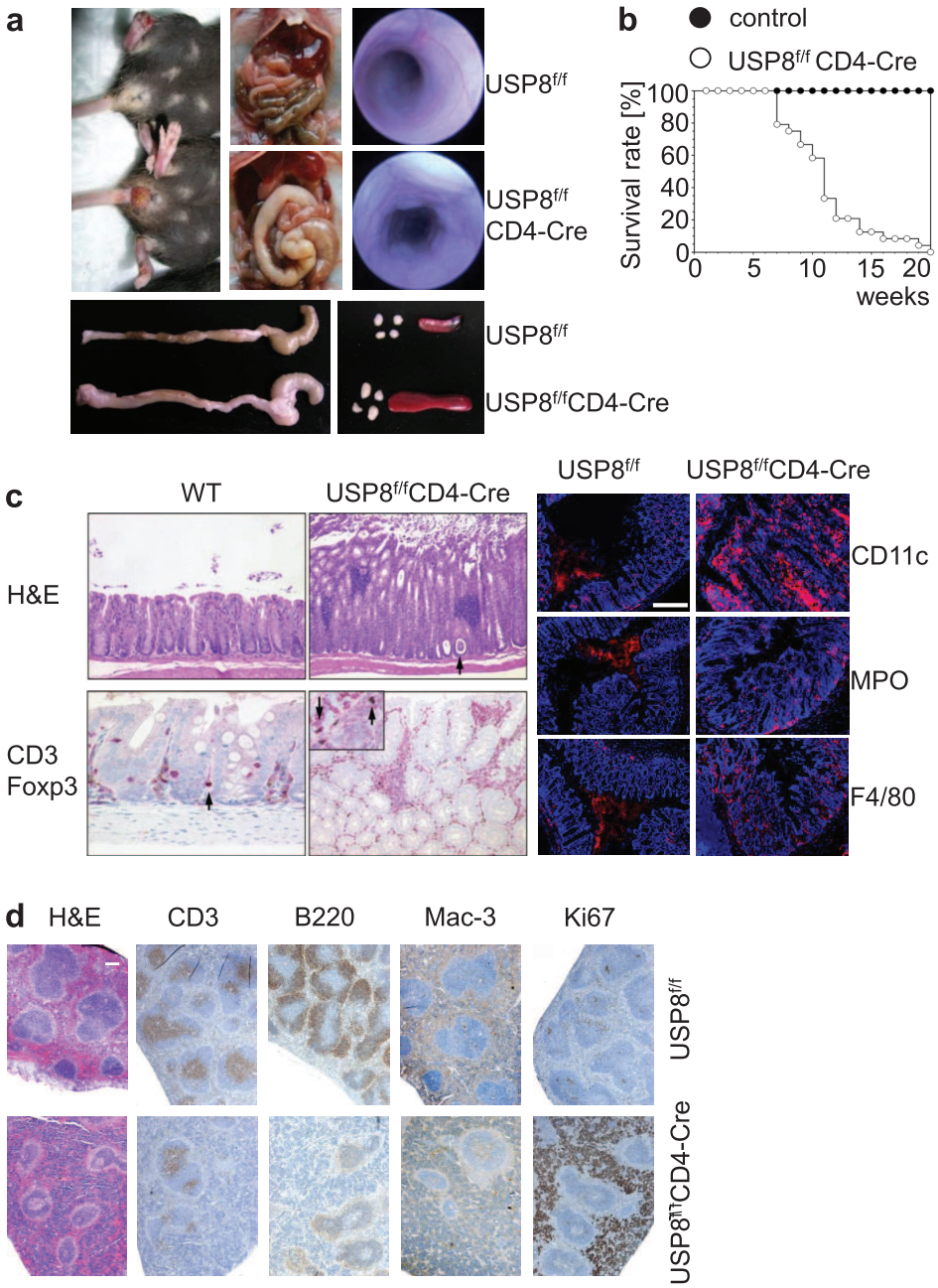

Dufner et al., Fig. 6

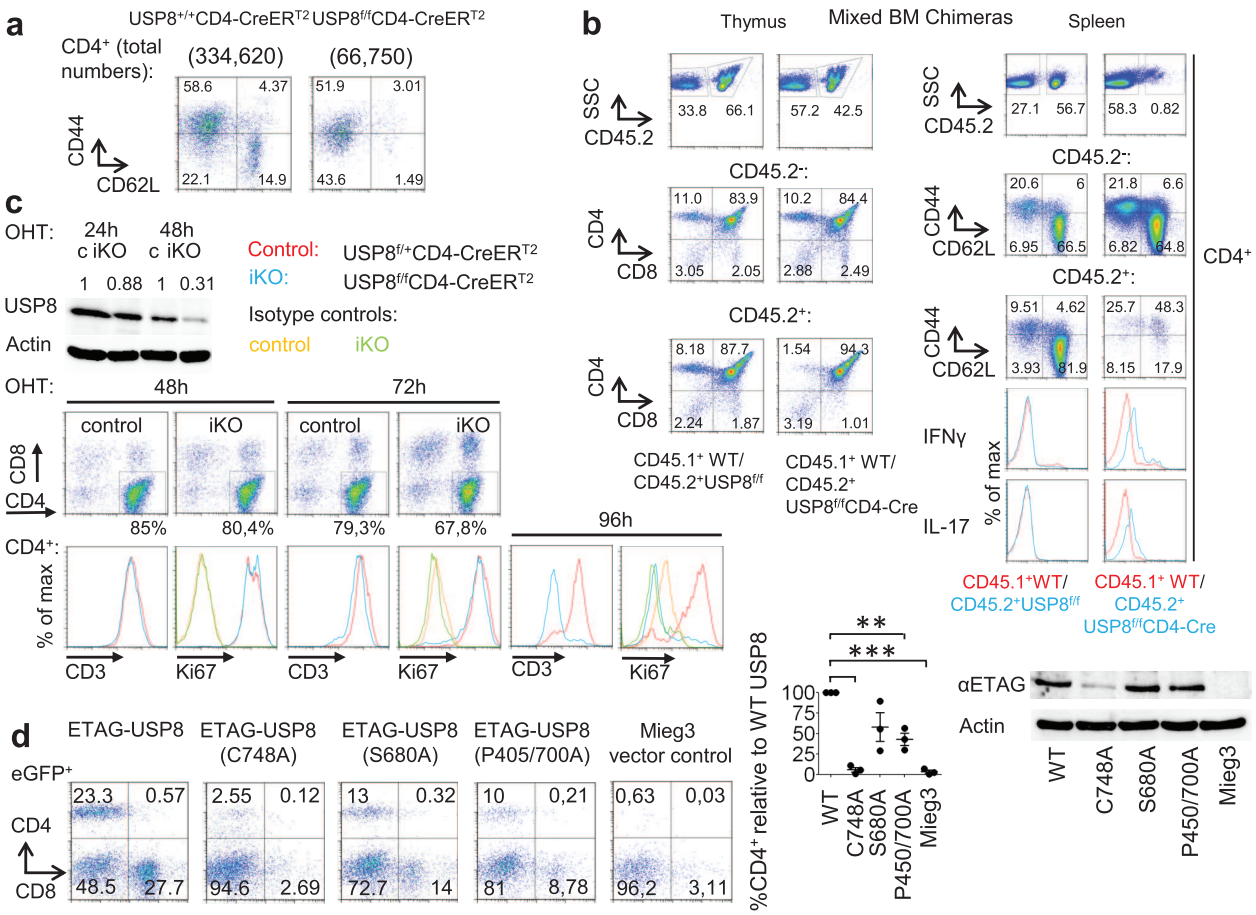

Dufner et al., Fig. 7

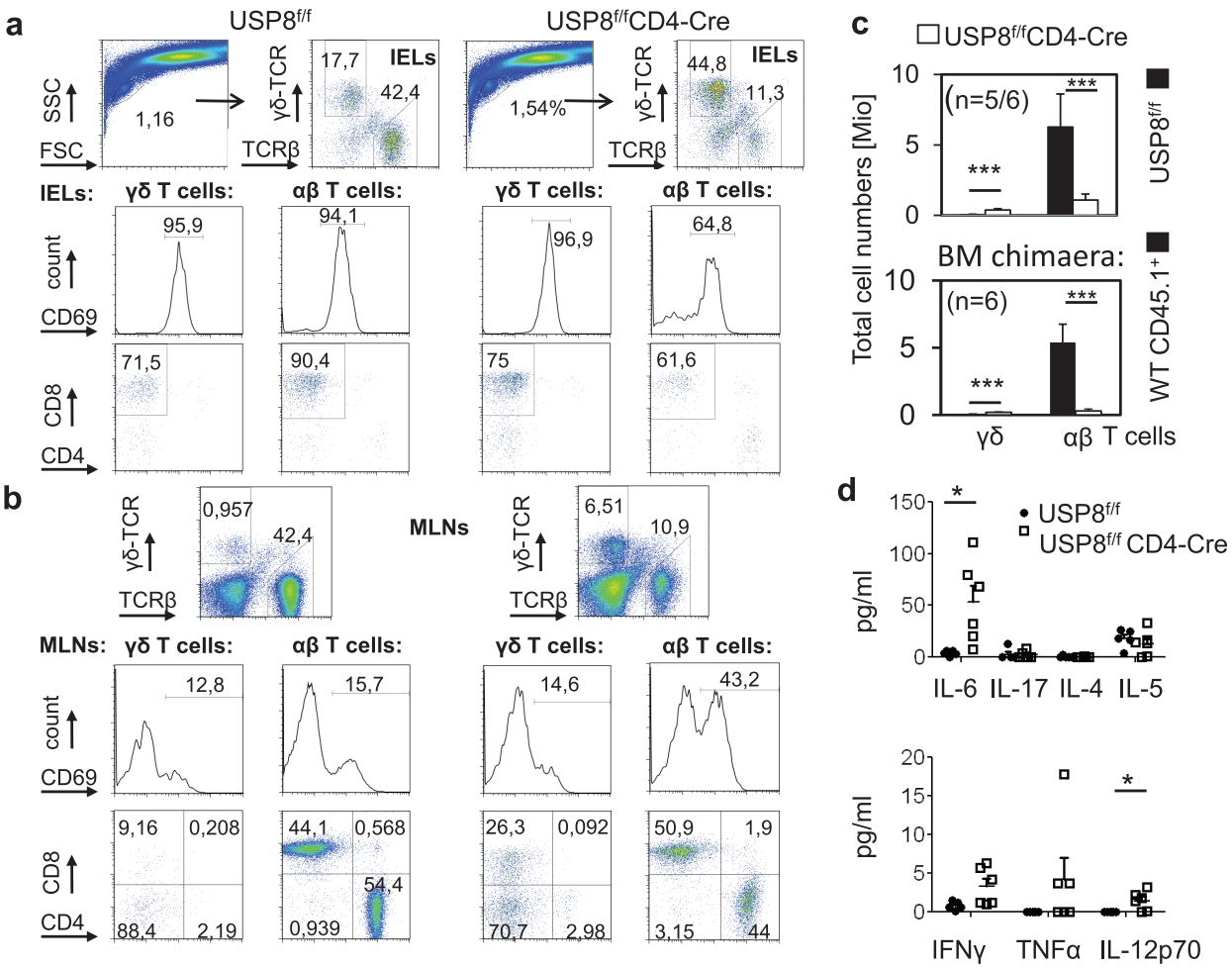

Dufner et al., Fig. 8

Yeast 2-hybrid

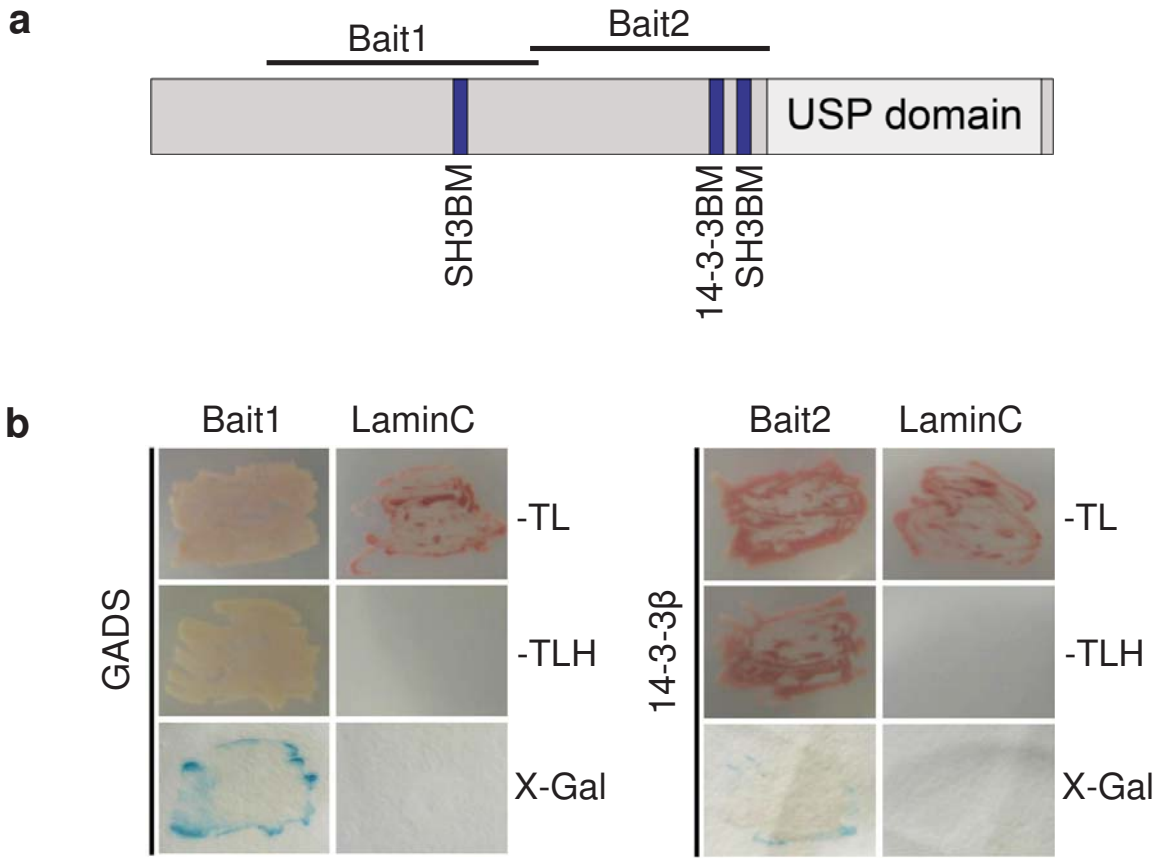

Dufner et al., Fig. S1

a

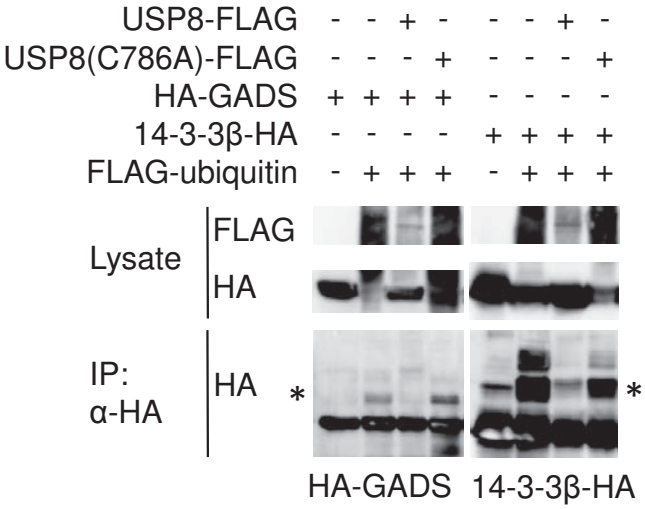

b

14-3-3β ubiquitination sites:

K9

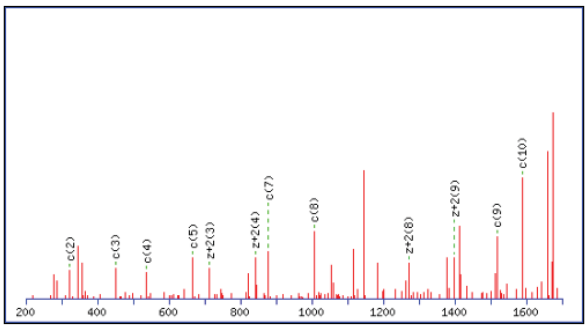

Monoisotopic mass of neutral peptide Mr(calc): 1716.9192
Variable modifications:
N-term : Acetyl (N-term)
M1 : Oxidation (M)
K9 : Ubiquitin LRGG (K)
Ions Score: 35 **Expect:** 0.3

MDKSELVQKAK

K189

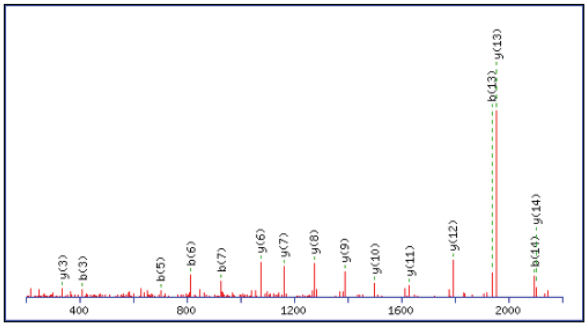

Monoisotopic mass of neutral peptide Mr(calc): 2202.0779
Variable modifications:
K12 : Ubiquitin LRGG (K)
C14 : Carbamidomethyl (C)
Ions Score: 59 **Expect:** 0.001

VFYYEILNSPEKACS

Dufner et al., Fig. S2

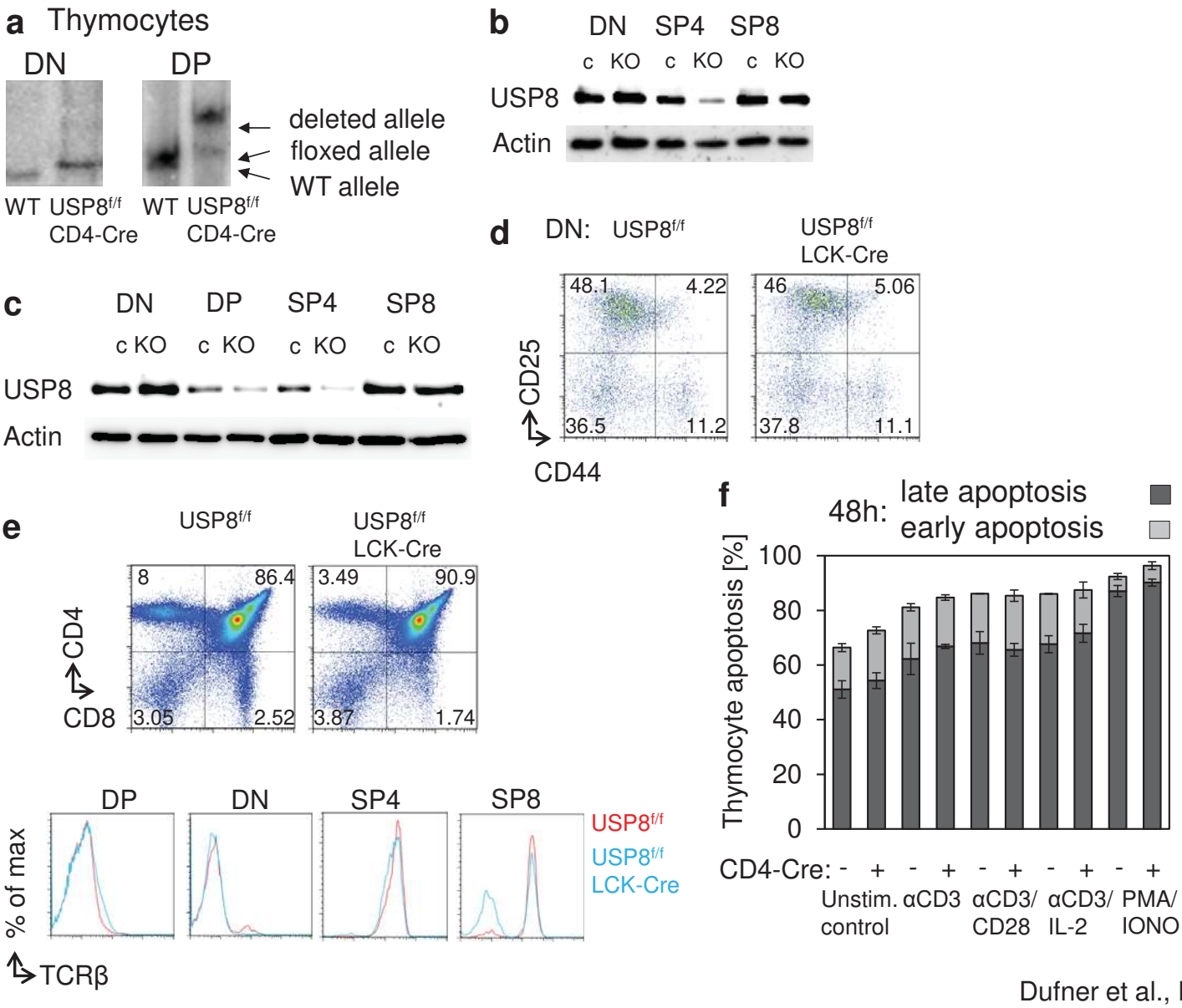

Dufner et al., Fig. S3

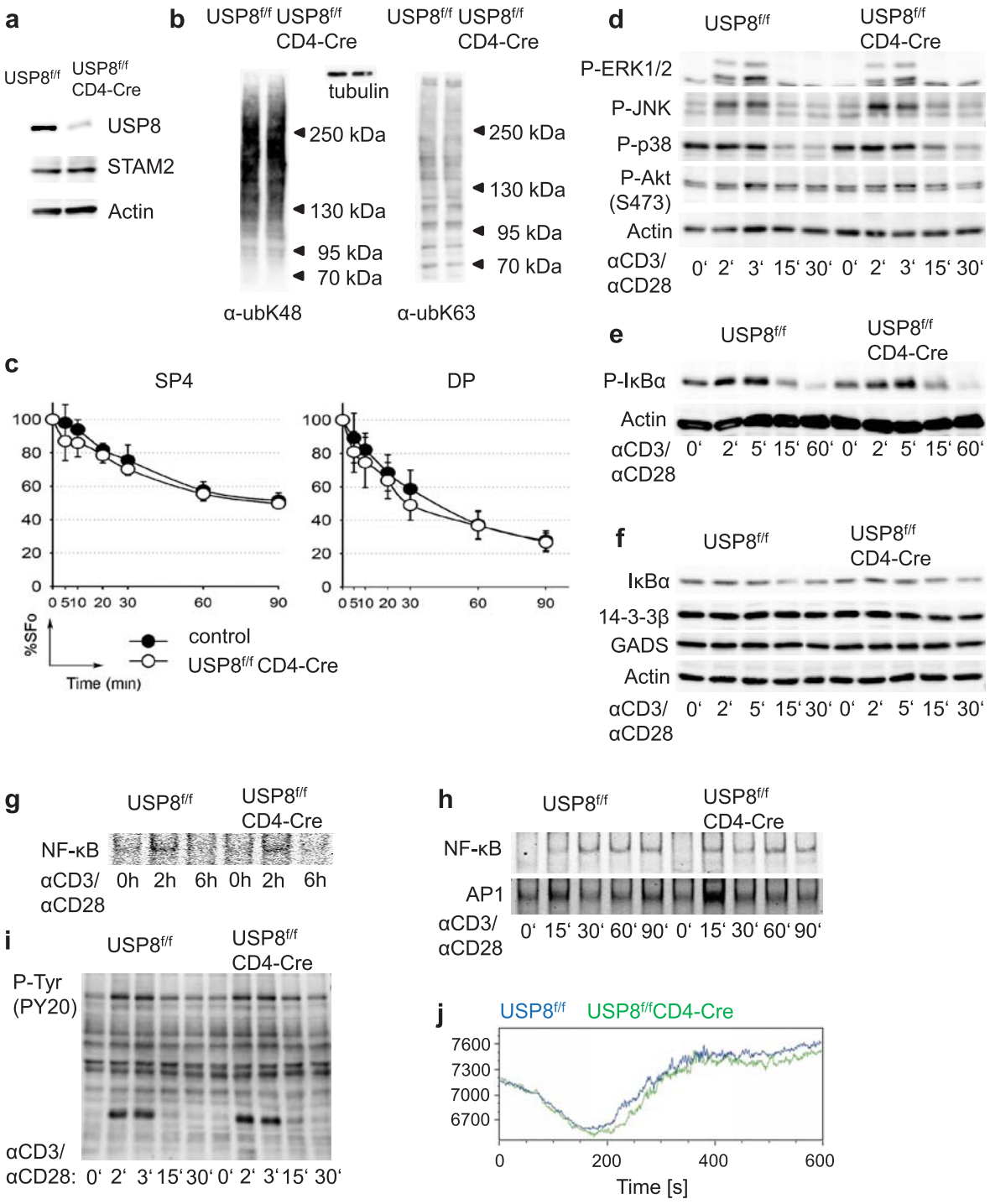

Dufner et al., Fig. S4

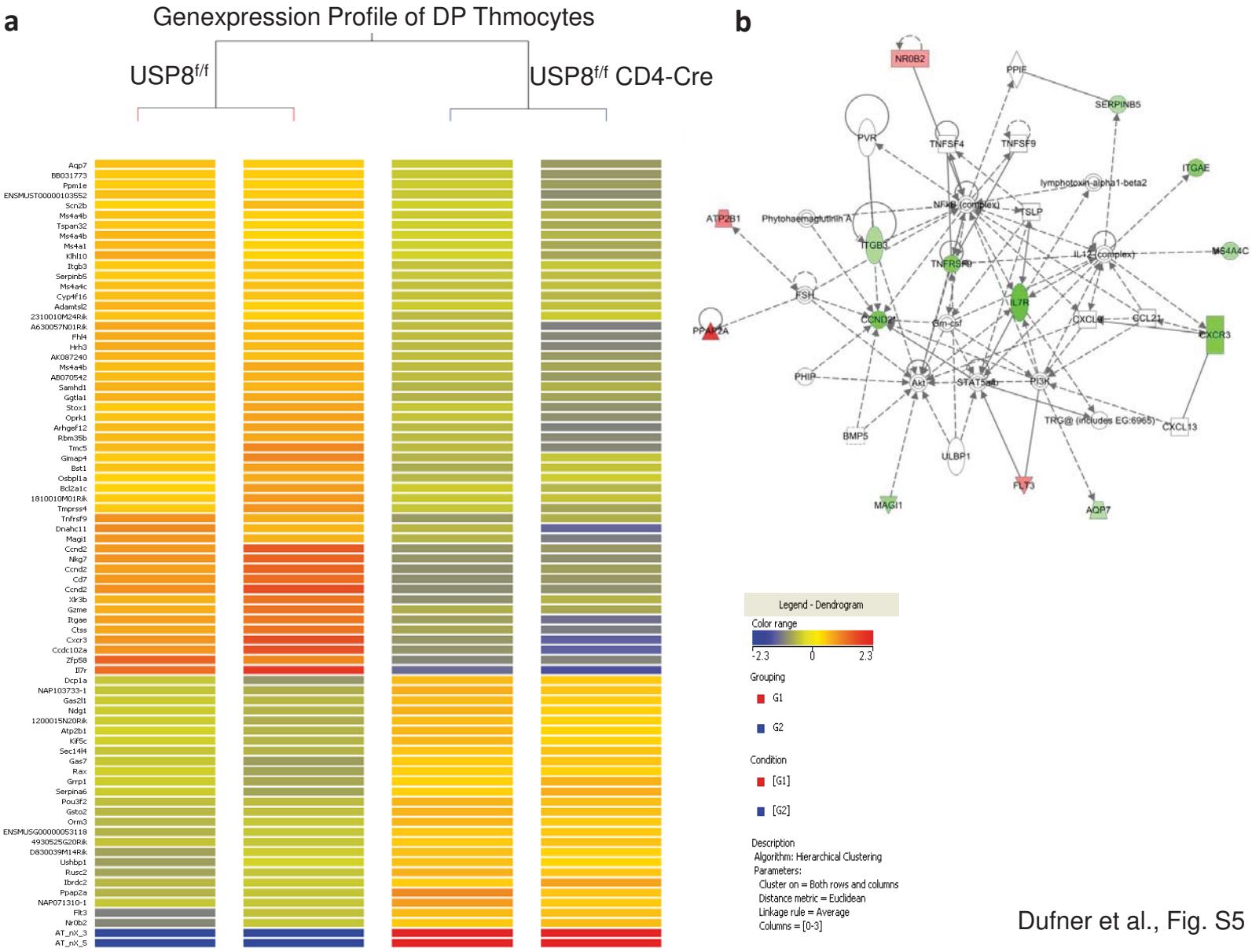

Dufner et al., Fig. S5

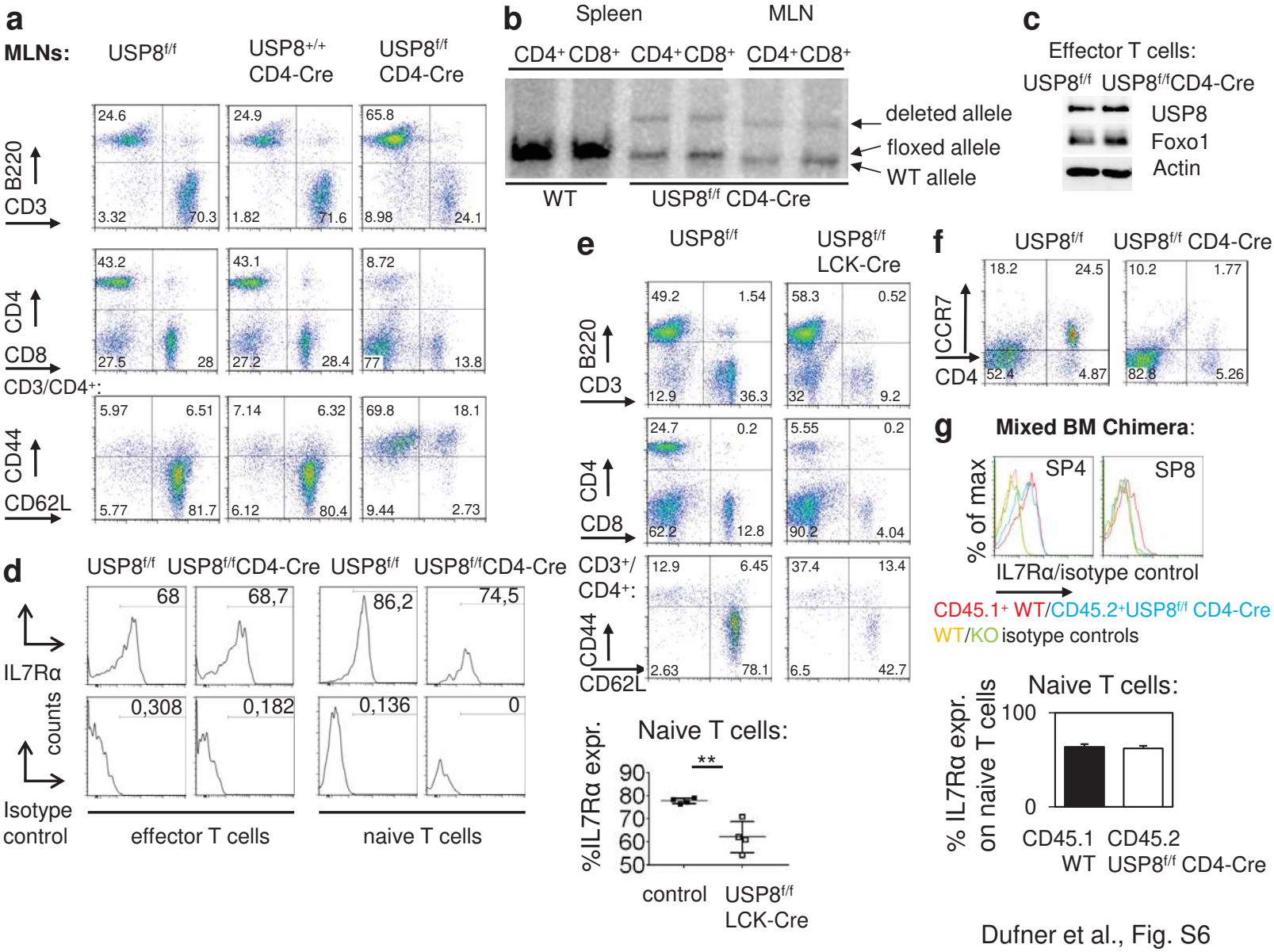

Dufner et al., Fig. S6

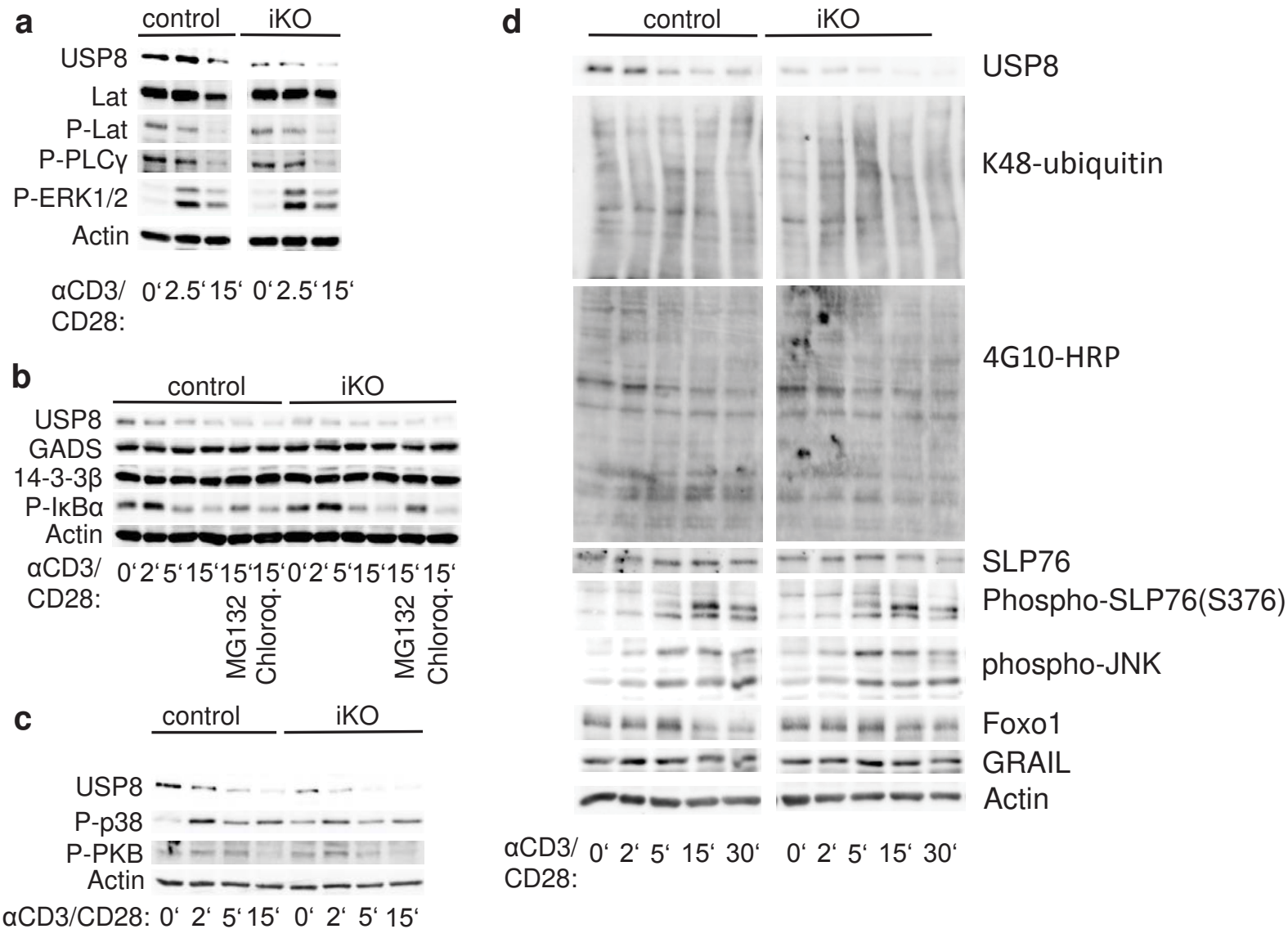

Dufner et al., Fig. S7

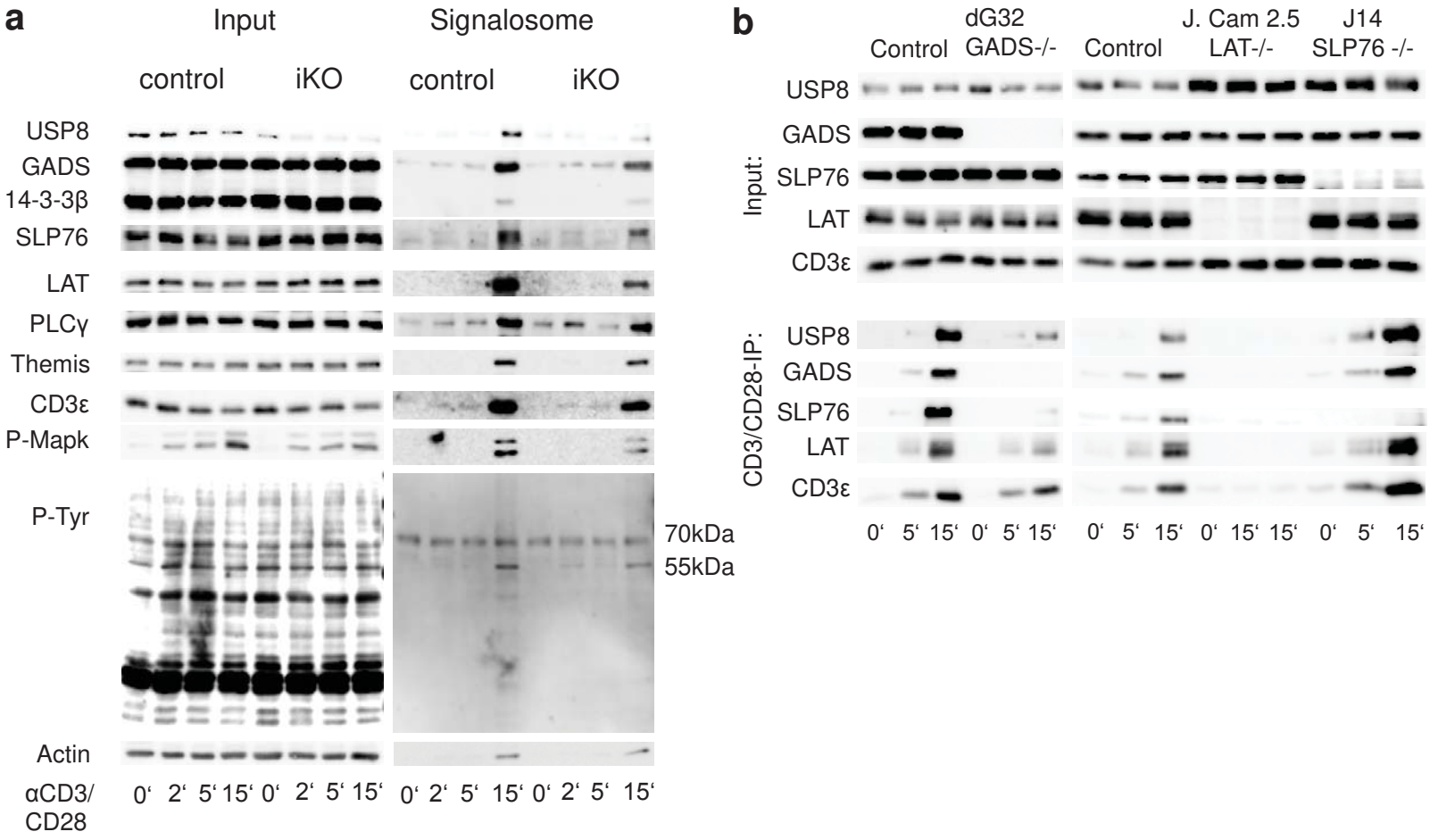

Dufner et al., Fig. S8